Received: 15 January 2024 | Revised: 12 June 2024 | Accepted: 24 June 2024

DOI: 10.1111/bre.12885

Basin Research IAS EAGE WILEY

RESEARCH ARTICLE

New insights into the structural and stratigraphic evolution of the Malay Basin using 3D seismic data: Implications for regional carbon capture and storage potential

Iain de Jonge-Anderson[1] | **Ana Widyanita**[1,2] | **Andreas Busch**[3] | **Florian Doster**[1] | **Uisdean Nicholson**[1]

[1]Institute of GeoEnergy Engineering (IGE), School of Energy, Geoscience, Infrastructure & Society, Heriot-Watt University, Edinburgh, UK

[2]PETRONAS Research Sdn. Bhd, Bandar Baru Bangi, Malaysia

[3]Lyell Centre, Heriot-Watt University, Edinburgh, UK

Correspondence
Iain de Jonge-Anderson, Institute of GeoEnergy Engineering (IGE), School of Energy, Geoscience, Infrastructure & Society, Heriot-Watt University, Edinburgh EH14 4AS, UK.
Email: i.anderson@hw.ac.uk

Abstract

The Malay Basin is a mature hydrocarbon province currently being re-assessed for CO_2 storage. Selecting an appropriate storage site requires a comprehensive understanding of the structural and stratigraphic history of the basin. However, previous studies have been limited to observations from either regional 2D seismic lines or individual 3D seismic volumes. In this study, we access and utilise a basin-wide (ca. 36,000 km^2) 3D seismic and well database to describe the structural and stratigraphic features of the basin, particularly those within the uppermost ca. 4 km (Oligocene to Recent) and gain new insights into the basin's evolution. E–W transtensional rift basins first developed due to sinistral shear across an NW-SE strike-slip zone. The NW-SE basin morphology seen today was generated during the late Oligocene–early Miocene, during which time dextral motion across marginal hinge zones created en-echelon antithetic, extensional faults and pull-apart basins, especially well preserved along the western margin of the basin. Collisional forces to the southeast during the early to middle Miocene resulted in the shallowing of the basin, intermittent connection to the South China Sea and a cyclic depositional pattern. Around 8 Ma (late Miocene), a significant uplift of the basin resulted in a major unconformity with up to 4.2 km of erosion and exhumation in the southeast. In the centre and northwest of the basin, the inversion of deeper E–W rifts resulted in the folding of Miocene sequences and the formation of large anticlines parallel to the rift-bounding faults. The Pliocene to Pleistocene history is more tectonically quiescent, but some extensional faulting continued to affect the northwest part of the basin. Larger glacio-eustatic sea-level fluctuations during this time resulted in major changes in sedimentation and erosion on the Sunda Shelf, including the formation of a middle-Pliocene unconformity. These structural events have created a variety of hydrocarbon traps across the basin of different ages, including transpressional anticlines, rollover anticlines and tilted

fault blocks. Each of these has discrete and distinct trap elements with important implications for their CO_2 storage potential.

1 | INTRODUCTION

The geodynamic history of Sundaland and the structural evolution of Cenozoic rift basins located on it have been the subject of many scientific studies in the past. The evolution of these basins is influenced by various important regional geological events, including the Indian-Eurasian collision, the opening of the South China Sea and subduction/collision along various plate boundaries (Figure 1a; Doust & Sumner, 2007; Hall & Morley, 2004; Hall et al., 2009; Metcalfe, 2011, 2017; Morley, 2002; Pubellier & Morley, 2014). Despite this increase in our understanding of the tectonic boundary conditions at the plate level, a detailed understanding of the evolution of these basins is limited. This is despite the fact that many of these basins have been extensively explored for hydrocarbons, resulting in vast geophysical and geological datasets associated with drilling.

The largest of these basins is the Malay Basin, which is around 500 km long, 200 km wide, 12 km deep and strikes NW-SE, roughly parallel with the Malay Peninsula (Figure 1b). It lies in coastal waters less than 100 km from the Malaysian shoreline, but its northwest, northeast and southeast margins extend into waters belonging to Thailand, Vietnam and Indonesia, respectively. It is bound by basement highs to the southwest (Terengganu Shelf) and northeast (Khorat Swell) that eventually rise to crop out onshore, where they form the Malay Peninsula and Vietnamese/Cambodian coast of the Southeast Asian landmass, respectively. To the northwest, it is separated from the Pattani Basin by the Narawathi High (Figure 1b). To the southeast, it is separated from the Penyu and West Natuna Basins by the Tenggol Arch and the southern promontory of the Khorat Swell, respectively (Figure 1b).

It is a prolific petroleum basin (Madon, 2021; Rice-Oxley & Abu-Bakar, 2022), hosting over 181 discoveries and over 14.8 billion barrels of oil equivalent (bboe) in recoverable resources (Madon, 2021). Therefore, most scientific understanding of its stratigraphy and structure comes from activities associated with the exploration, appraisal and development of hydrocarbon resources. Early stratigraphic frameworks for the basin were published by Woolands and Haw (1976), Armitage and Viotti (1977), Ramli (1988) and Yakzan et al. (1996), all of which describe the different schemes adopted by the various companies that have explored the region. Early insights into the structure of the basin were published by Kuang (1988) and Ng (1987), but the first detailed accounts were published in studies reporting on seismic data analysis during the mid to late 1990s. These accounts initially focused on the evidence for strike-slip deformation and structural inversion within the basin, particularly along its western flank (Liew, 1994; Tjia, 1994; Tjia & Liew, 1996). These were followed by a series of publications that defined the basin's broader structural framework and kinematic history by integrating seismic, gravity and magnetic datasets (Liew, 1997; Madon, 1997; Madon & Watts, 1998; Ngah et al., 1996).

Highlights

- Newly available 3D seismic data used to reconstruct the structural and stratigraphic evolution of the Malay Basin highlighting key episodes of faulting, graben development and inversion.
- Structural features include deep Paleogene grabens, Oligocene-Miocene strike-slip shear zones, transpressional folding and a deep Miocene–Pliocene unconformity.
- These produce a range of structural traps that could be utilised for future CO_2 storage projects.

More recently, scientific focus has shifted to understanding the petroleum system (Bishop, 2002; Doust, 2017; Doust & Sumner, 2007; Madon et al., 2006; Nayak et al., 2023; Petersen et al., 2011), overpressure (Ahmed Satti et al., 2016; Madon, 2007; Tingay et al., 2011, 2013), subtle stratigraphic and structural features at either the field-scale (Almasgari et al., 2020; Babikir et al., 2022; Hou et al., 2008) or the regional scale (Alqahtani et al., 2015, 2017; Miall, 2002) and the emerging basement hydrocarbon play (Madon et al., 2020). The only recent regional reassessment of the geological structure is that of Mansor et al. (2014), who used insights from the interpretation of deep (8000 ms TWT, two-way-time) regional 2D lines to describe the basement structure and fault patterns.

The Malay Basin is also considered to be an important area for future carbon capture and storage (CCS; Abd Rahman et al., 2022; Hasbollah et al., 2020). However, these studies employ relatively broad evaluations of subsurface geology in their analyses. The Malay Basin contains numerous mature fields that could be re-purposed for the geological storage of CO_2, offering an abundance of data and production history. Still, their potential is hindered by limited storage capacity, field availability and

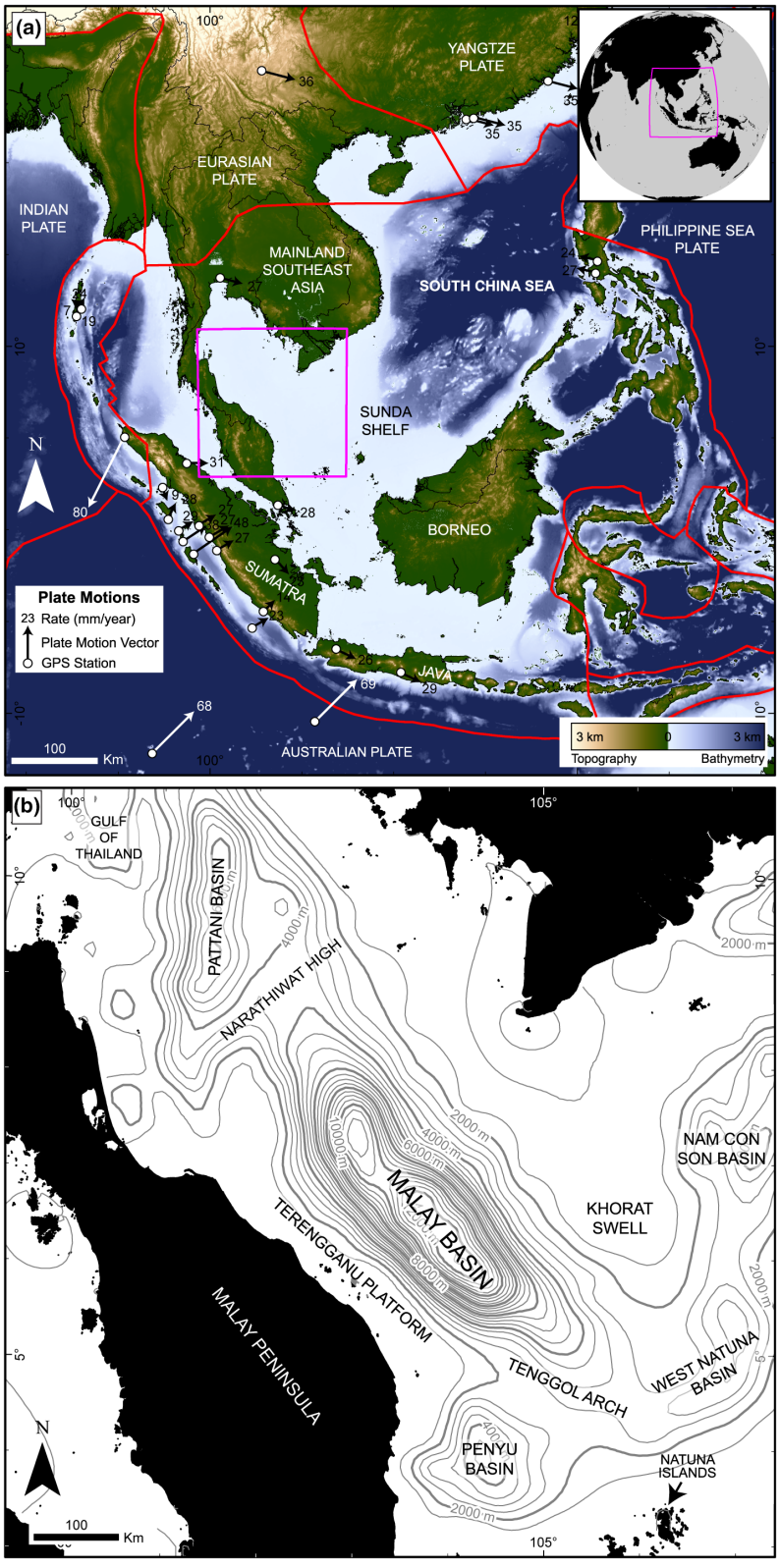

FIGURE 1 (a) Map of southeast Asia highlighting bathymetry and topography (GEBCO Compilation Group, 2023), plate boundaries (Argus et al., 2011; Bird, 2003) and GPS-derived horizontal plate motions (Heflin et al., 2020). (b) Map of the waters between the Malay Peninsula and mainland southeast Asia highlighting the offshore total sediment thickness (Straume et al., 2019) and locations of major basins and highs.

pressure changes following depletion. There is currently insufficient capacity within Malay Basin depleted fields to meet the Malaysian government's CO_2 storage ambitions. Hence, it is important to study other storage site types, one of which is saline aquifers. However, there is often significantly less information available for saline aquifers, particularly regarding reservoir/caprock distribution and the presence of structural traps.

This study was motivated by the need to better understand the distribution of potential CCS traps and their associated risks across the Malay Basin. To achieve this, a comprehensive evaluation of the basin's structure and

stratigraphy was undertaken. The aims were to achieve a better understanding of geological events affecting the basin (and the wider SE Asia region) and to determine the timing of traps for CO_2 storage and their present-day spatial distribution. Key to this was the interpretation of an extensive 3D seismic database that has not been utilised in previous studies of the basin.

2 | GEOLOGICAL SETTING

2.1 | Structural setting

The basin lies on the Sunda Shelf, a region of shallow water (<100 m) that is located between mainland southeast Asia, the Malay Peninsula and the large islands of Sumatra, Java, and Borneo (Figure 1a,b). The shelf has undergone multiple cycles of emergence and submergence since 400 ka (McGrath et al., 2023; Sarr et al., 2019), and while emergent, formed an expansive, linked biogeographical and geological system across Southeast Asia, referred to as Sundaland. The continental core of Sundaland, the Sunda Plate, was assembled during the Mesozoic and is the result of the closure of multiple Tethyan oceans and the amalgamation of continental fragments derived from the India-Australian margin of eastern Gondwana (Hall et al., 2009; Hall & Morley, 2004; Metcalfe, 2009, 2011; Morley, 2012). To the west, south and east, the plate is bounded by complex and tectonically active regions, following the subduction of the Indian, Australian and Philippine Sea plates, respectively (Figure 1a).

The Malay Basin is one of several continental rift basins that lie on the west of Sundaland, extending from the Gulf of Thailand down to the Natuna Islands (Figure 1b). Extension across the area now occupied by the Malay Basin began during the late Eocene (Hall & Morley, 2004; Madon, 1997; Pubellier & Morley, 2014; Tjia, 1998), generating a pattern of E–W-striking faults and narrow basins (Figure 2) (Tjia, 2014; Tjia & Liew, 1996). This structural fabric was produced in a transtensional regime involving extension across a broadly NW-SE left-lateral (sinistral) shear zone, believed to be the offshore continuation of Three Pagodas and Mae Ping fault zones (Doust & Sumner, 2007; Fyhn et al., 2010; Madon, 1997; Mansor et al., 2014). It is widely held that this strike-slip zone was activated during the latest Eocene following the collision of the Indian and Asian continents and the lateral extrusion of rigid continental blocks (such as the Sunda Plate)

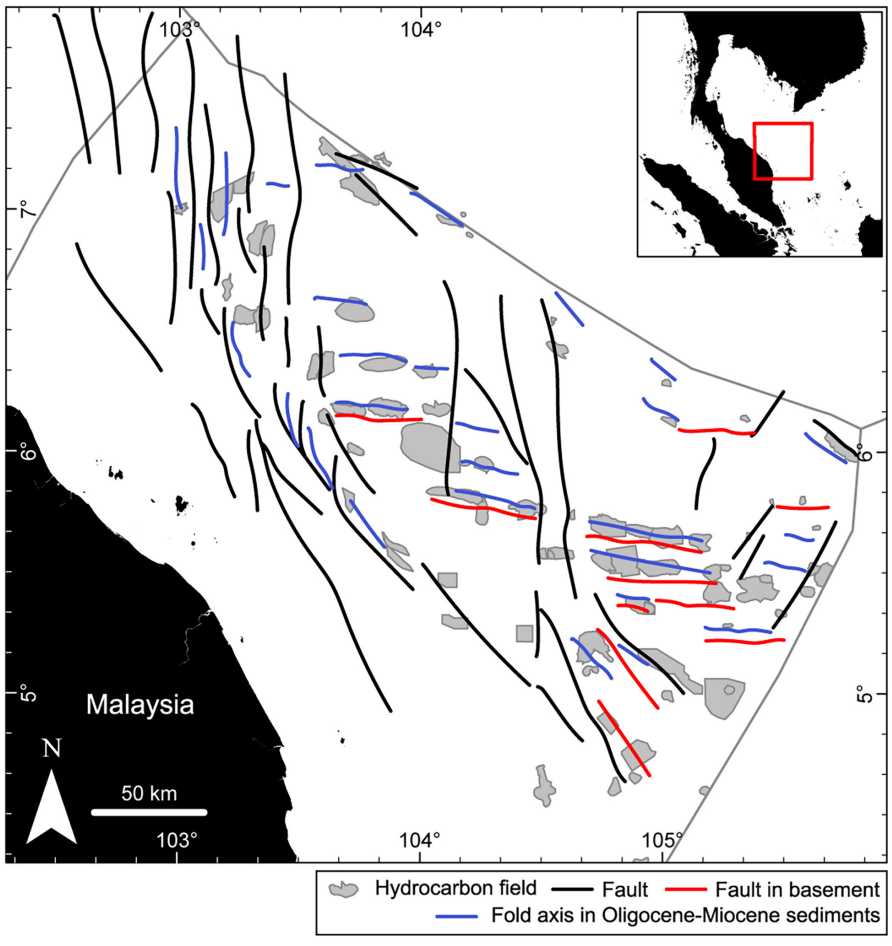

FIGURE 2 Major structures in the Malay Basin (after Tjia & Liew, 1996).

to the southeast (Molnar & Tapponnier, 1975; Pubellier & Morley, 2014; Tapponnier et al., 1982).

The Malay Basin continued to open during the Oligocene, with dextral movement along basin-margin hinge zones (e.g., Western Hinge Fault Zone; Tjia, 1994). These hinge zones strike NW-SE, and their development has been linked to either the Three Pagodas Fault Zone, or rollback associated with the subduction of the Indian plate oceanic crust (Morley, 2002; Pubellier & Morley, 2014). Lateral motions across these faults initially created small pull-apart basins along the hinge zones that would be the loci for pre-late Oligocene sediments before the basin widened and opened fully (Tjia, 1994). Continued shearing produced roughly NW-SE-striking faults that linked both hinge zones and created a fabric of NNW–SSE-striking sub-basins and highs within the basin (Mansor et al., 2014).

Miocene compression caused the uplift and inversion of many Sundaland rift basins, particularly those located along its southern margin (Doust & Sumner, 2007; Pubellier & Morley, 2014). Inversion structures associated with these uplift events are evident in the West Natuna Basin, where several small early-middle Miocene unconformities and a more prominent, middle-late Miocene unconformity have also been documented (Ginger et al., 1993). The latter is a local expression of the widespread middle Miocene unconformity (MMU), which marked the end of seafloor spreading in the South China Sea at 16 Ma (Hutchison, 2005). In the Malay Basin, this event is represented by a prominent late Miocene (Tortonian) unconformity referred to as the 'Intra-Late Miocene Unconformity' (Ramli, 1988) or the 'Upper Miocene Unconformity' (UMU; Yakzan et al., 1996). Its development has been attributed to the reversal in slip sense along NW-SE strike-slip faults and the inversion of pre-existing W-E-oriented depocentres (Tjia, 1998).

A smaller, 'Top Middle Miocene Unconformity' also exists, where the lower part of Group E is missing at the southeast part of the basin (Yakzan et al., 1996). This has been attributed to a major relative sea-level fall across the area (Yakzan et al., 1996). This unconformity is difficult to identify in the Malay Basin, particularly as it was subsequently overprinted by the UMU over much of the basin. However, early Miocene unconformities have been described within the West Natuna Basin (Ginger et al., 1993), and various compressional events have been noted during this time including continental collision along the southeast margin of Sundaland (Doust & Sumner, 2007; Morley et al., 2003; Pubellier & Morley, 2014) and the collision of the Dangerous Grounds with Borneo (Clift et al., 2008; Hutchison et al., 2000).

The Malay Basin, and the wider region, experienced little tectonic activity during the Pliocene and Pleistocene. The Pattani Basin, in the north, was not affected by late Miocene inversion and, instead, has been steadily subsiding since the early Miocene (Bustin & Chonchawalit, 1995). In the southeast, following significant structural inversion, the West Natuna Basin experienced a renewed phase of subsidence (Ginger et al., 1993), which has tentatively been linked to the termination of the rotation of Borneo (Morley et al., 2003).

2.2 | Stratigraphy

There are several stratigraphic nomenclatures used to describe the Cenozoic sediments within the Malay Basin (Armitage & Viotti, 1977; Ramli, 1988; Woolands & Haw, 1976; Yakzan et al., 1996). However, the main subdivisions are fundamentally the same (Figure 3). The first basin-wide scheme was proposed by Esso, in which 'Groups' are given alphabetical notation (A-M) based on seismic characteristics (Madon, Karim, et al., 1999). This scheme was later adjusted following a revised biostratigraphic framework for the basin (Yakzan et al., 1996). This notation is the most frequently used scheme within the basin and is adopted for this study, though other schemes are presented in Figure 3 for reference.

While the oldest sediments drilled within the basin are Oligocene in age, seismic and biostratigraphic observations from adjacent areas imply an older, middle-late Eocene age date for the formation of the basin (Fyhn et al., 2010; Kessler et al., 2021). Since this initial opening, over 14 km of sediments are estimated to have been deposited in the centre of the basin (Arshad et al., 1995). Because of the thick sedimentary cover, the current understanding of the oldest sediments is almost exclusively from the southeast flank of the basin, where structural inversion and limited post-rift subsidence have resulted in these sediments being at depths still feasible for drilling (3–4 km). These sediments belong to the Oligocene (Rupelian to Chattanian) Groups M and L, equivalent to the Ledang and Seligi formations (Figure 3). Both groups consist of basal sandstones capped by a thick shale (Yakzan et al., 1996). The shale at the top of Group M (Ledang Shale) was deposited in freshwater lacustrine conditions (Yakzan et al., 1996). However, there is debate about the depositional environment of Group L (Seligi Shale). Some authors note the presence of marine foraminifera (Armitage & Viotti, 1977; Yakzan et al., 1996), but Lunt (2021) suggested these were likely caved samples that collapsed into boreholes from shallower stratigraphic intervals and that nonmarine conditions persisted throughout Group L. The sandstones are interpreted to be deposited in an alluvial fan environment by braided fluvial systems and distributary mouthbars (Jumari et al., 2011; Rosly et al., 2019; Yusak, 2012).

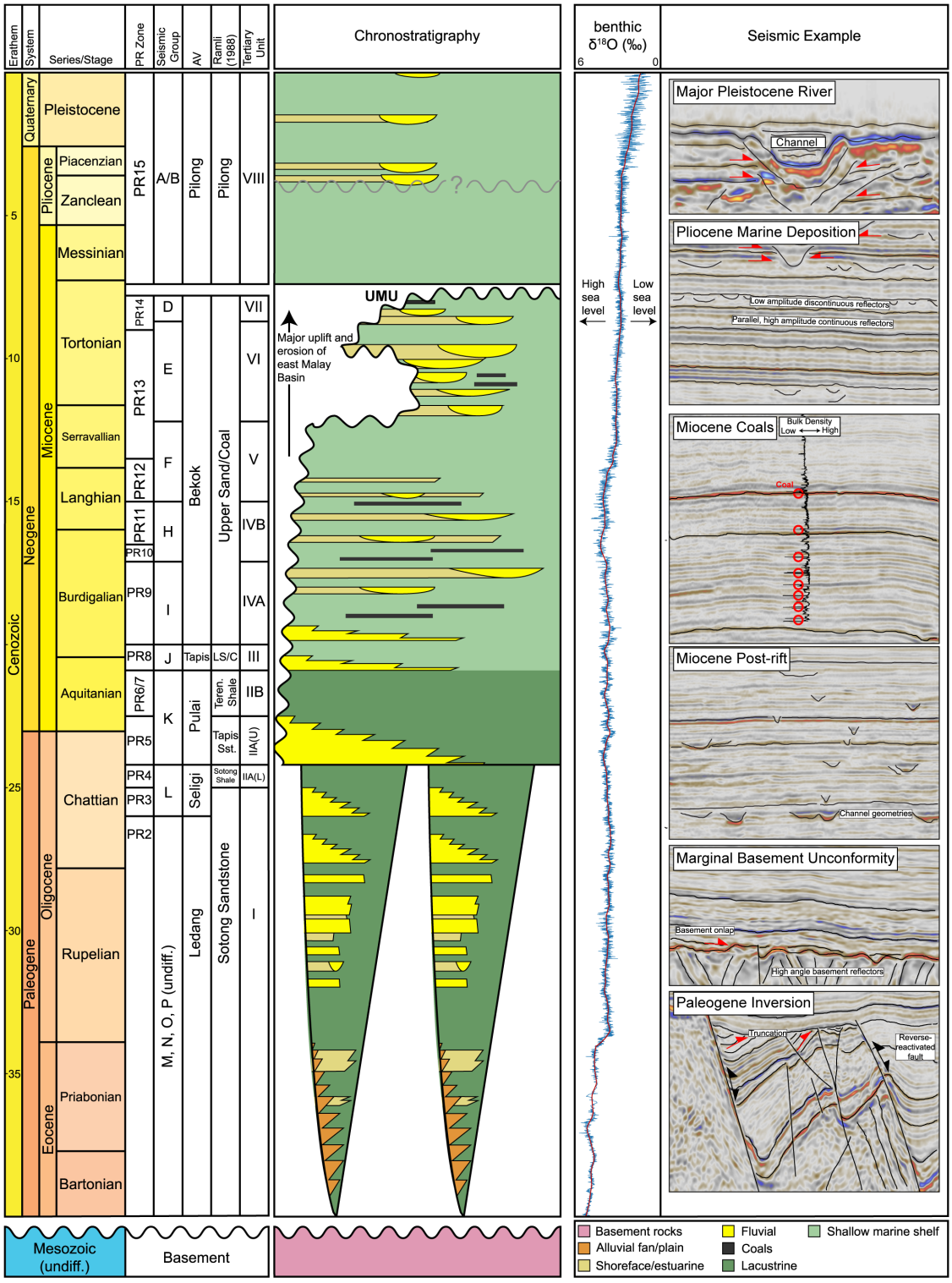

FIGURE 3 Stratigraphic chart for the Malay Basin (after Armitage & Viotti, 1977; Lunt, 2021; Madon, Abolins, et al., 1999, Madon, Karim, et al., 1999; Mansor et al., 2014; Ramli, 1988; Yakzan et al., 1996). Oxygen isotope data is after Westerhold et al. (2020). AV: Armitage and Viotti (1977), LS/C: Lower Sand/Coal, PR: Palynomorph assemblage zones (Yakzan et al., 1996), Teren.: Terengganu.

The upper Oligocene (Chattanian) to lower Miocene (Aquitanian) Group K has been drilled extensively along the basin margins and in more central, inverted areas. It consists mainly of a lower sequence of braided fluvial/deltaic sandstones and an upper, thick shale. The upper shale ('K Shale') is an important unit in which palynological indicators suggest a transition from land-locked lacustrine deposition to nearshore freshwater swamps

(Lunt, 2021) with increasingly brackish waters (Armitage & Viotti, 1977).

A shift in tectonic regime from rifting to thermal subsidence occurred at the start of the Miocene during which the basin also experienced its first marine incursion (Yakzan et al., 1996). The basin lay at or near sea level, with much of the area covered by a lower coastal plain, with fluvio-deltaic systems draining basement highs to the southwest (nearshore Peninsular Malaysia) and northeast (Khorat Swell) (Madon, Abolins, et al., 1999; Ramli, 1988). Groups J and I were deposited during the early Miocene (Aquitanian to Burdigalian) within mainly a brackish to shallow marine setting (Shing, 1992).

Lower Miocene sandstones form reservoirs within many oil and gas fields, and several published works have described their sedimentological characteristics from core extracted from these fields. These recognise distinct depositional facies including tidally reworked subtidal bars, estuarine channel sands, storm-related sheet flood sandstones and offshore marine shales (Madon, Karim, et al., 1999; Ramli, 1988; Thye, 1996). During this period, the emerging West Natuna block intermittently created a sill that restricted marine waters from entering the Malay Basin from the east. This effect, superimposed on sea-level fluctuations, resulted in a Miocene sequence composed of various transgressive-regressive periods and cyclic deposition (Jirin et al., 2013; Madon, 2011).

The middle Miocene Group F is composed almost entirely of mudstone, with a minor, middle sandstone unit (Yakzan et al., 1996). It also forms a pressure seal across the centre of the basin, with significant overpressure below (Madon, 2007). The lower part of this unit corresponds with a period of high regional sea level (Figure 3).

The top of Group F is marked by an unconformity that has removed part of Group E from the southeast of the Malay Basin (Figure 3). A sea-level fall during the middle-late Miocene resulted in a basin-wide regression and the development of a major, southerly-flowing fluvial/delta system along the axis of the basin (Madon, 1994). The result was the deposition of a thick (up to ca. 600 m) sequence of coastal plain to shoreface sediments in the lower part of Group E, which are overlain by a marine mudstone (Yakzan et al., 1996).

The Pliocene to Recent section of the Malay Basin has been less intensively studied, in part, because it is only a very minor reservoir interval for hydrocarbons (Madon, 2021). Early accounts of the stratigraphy describe an entirely marine section, consisting mainly of mudstone with occasional, thin coarser beds, referred to as the Pilong Formation (Armitage & Viotti, 1977). More recent analysis has suggested that the Pliocene can be sub-divided into a lower marine interval and an upper interval with greater non-marine influence, separated by a minor unconformity (Figure 3) (Lunt, 2021), which is also consistent with seismic geomorphological evidence (Miall, 2002). There was a steady drop in regional sea level throughout the Pliocene and Pleistocene, and the Sunda Shelf was permanently exposed to around 400 ka before experiencing repeated submersion-exposure cycles (McGrath et al., 2023; Sarr et al., 2019). During the Last Glacial Maximum lowstand, around 20 ka, a large river system developed, flowing from the Gulf of Thailand, through the Malay Basin and towards the South China Sea (Alqahtani et al., 2015, 2017; Miall, 2002; Twarog et al., 2021).

3 | DATA AND METHODOLOGY

The data underpinning this work comes from decades of hydrocarbon exploration, appraisal and production within the basin. Almost all of the basin has been covered by 2D and 3D seismic surveys (Madon, 2021), and an extensive 3D seismic dataset covering over 36,000 km^2 was available for this study (Figure 4).

The dataset consists of 10 seismic volumes of varying size and data quality. Record length varies from 4500 to 7500 ms TWT, and the sampling interval varies between 2 and 4 ms, and the inline/crossline spacing varies from 6.25 to 25 m. Many of these volumes are merged surveys, consisting of numerous smaller volumes already stitched together by a service company. The largest of these is 23,000 km^2 in area and covers most of the central part of the basin. There was no acquisition or processing information available other than those within file headers, and from visual inspection, it is evident that there are varying degrees of signal quality and post-processing filtering from survey to survey. Information on the polarity of the seismic data was also not provided, but from inspection of the seabed and basement reflectors, both of which are assumed hard interfaces, the polarity of the data was taken as positive, whereby these hard interfaces corresponded to seismic peaks (positive amplitudes).

A single velocity function was used to convert time-domain seismic interpretations to depth. To obtain this function, a quadratic function was fitted to all available checkshot data within the Malay Basin (Figure 5).

Previous studies addressing the structural evolution of the Malay Basin have been limited to observations from either individual 3D seismic datasets or regional-scale 2D seismic lines. Here, for the first time, we present an analysis of a basin-scale 3D seismic dataset. We started by mapping regional-scale seismic horizons across the entire dataset. These were calibrated by stratigraphic tops picked from wells with time-depth data (checkshots) available, and in some cases, synthetic seismograms were created to improve or quality-control the seismic-to-well tie. For

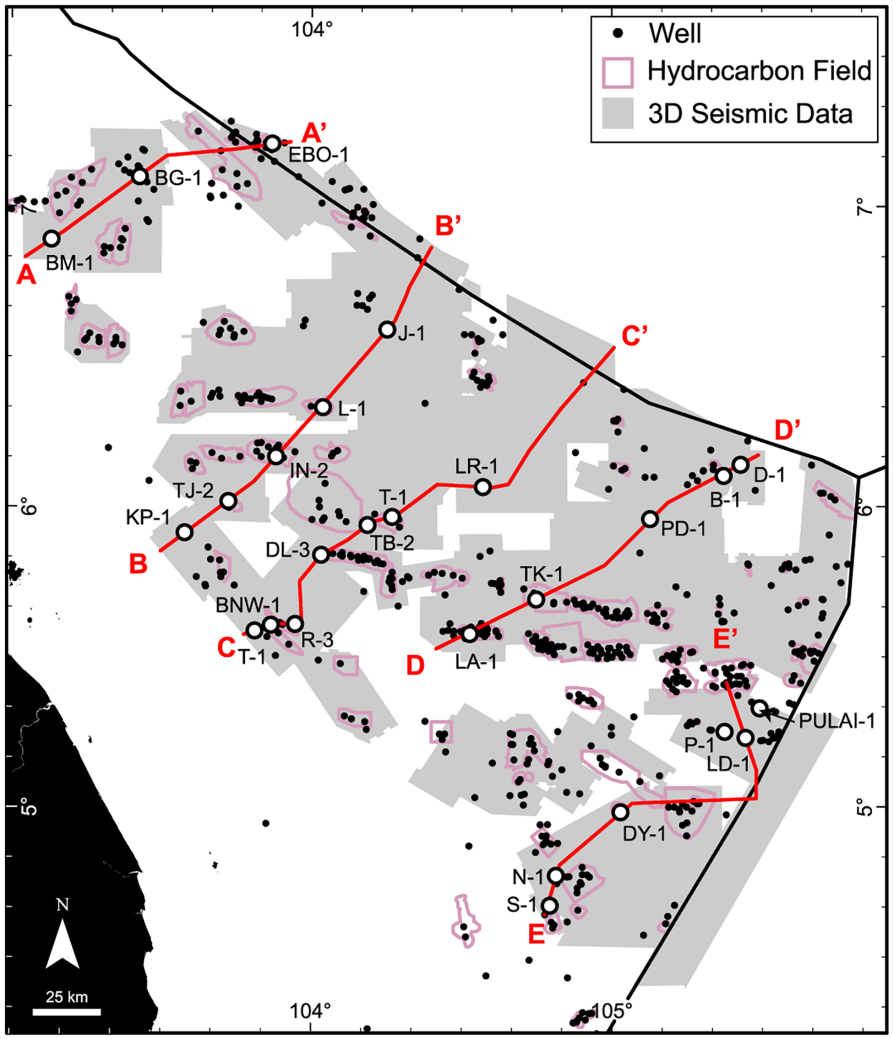

FIGURE 4 Map showing the outline of seismic and well datasets available for this study. Also shown are the locations of regional seismic cross-sections (Figure 7) and the locations of specific wells referenced in this study.

regional mapping, we concentrated on mapping the tops of each group (see subsequent section for an explanation of this nomenclature), but detailed top structure maps were also constructed for other, locally prominent intervals to describe key structural features in certain areas of the basin.

To aid the visualisation of geological structures, seismic variance maps were created for each time-structure map. Seismic variance is an attribute that measures trace-to-trace similarity over a given lateral and vertical window. In doing so, discontinuities are highlighted, which can often represent structural (e.g. faults) or stratigraphic (e.g. channel) features. We used a lateral window of three inlines by three crosslines and a vertical window of 15 traces for the variance computation. Once computed, these were draped on top of the time-structure surface with layer blending to allow visualisation of both.

The final step in our methodology was to review the trapping mechanisms for hydrocarbon discoveries within the basin. This was undertaken to determine the different trapping domains within the basin and relate these to the structural characteristics of the basin.

4 | RESULTS AND DISCUSSION

4.1 | Basin architecture

The seismic data available for our study allowed us to focus mainly on the central-to-southeastern part of the Malay Basin, offshore Malaysia (Figure 4). The basin structure is best illustrated with a basin-wide top structure map for a relatively deep lower Miocene horizon Group K (Figure 6) and long cross-sections along the main orientation of the structural dip (Figure 7).

The top basement horizon is a high amplitude, continuous to discontinuous seismic peak (downward increase in acoustic impedance) representing a major

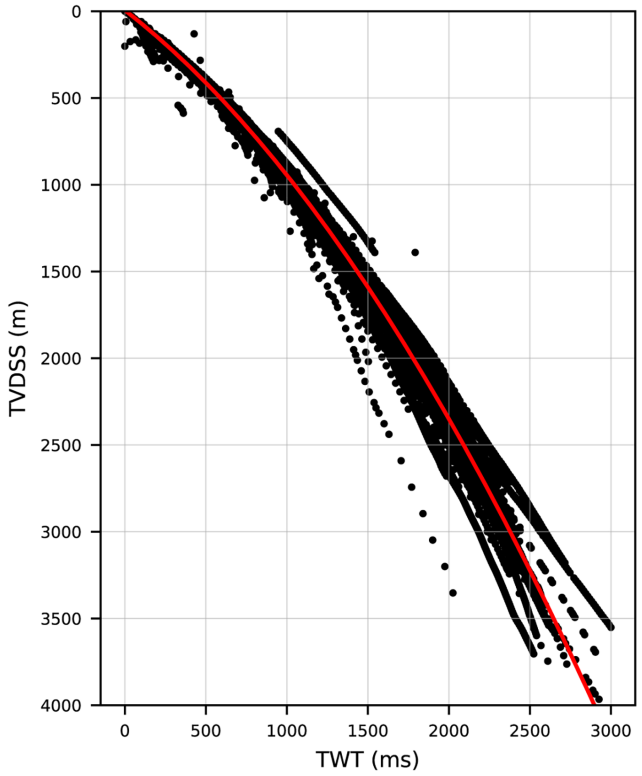

FIGURE 5 Plot of two-way-time (TWT) versus true vertical depth subsea for all checkshot data available within the Malay Basin. A quadratic function was fitted to the data to provide estimates of depth from time-based seismic interpretation.

unconformity separating folded Mesozoic rocks from the Cenozoic basin-fill succession (Figures 7 and 8). The internal seismic character of the basement itself is varied, ranging from folded, laterally continuous reflectors to chaotic, low-amplitude reflectors. Drilling results also support this, with various lithologies having been penetrated, including granites, clastics and carbonates (Madon et al., 2020). On the flanks of the basin, at depths of around 2000 ms TWT (2350 m) or less, the top basement reflector is high amplitude, continuous and easily traceable (Figures 7 and 8). At the southwest and northwest margins of the basin, there are deep faults that cut through the top basement horizon. In the footwall to these faults, the basement dips into the basin centre and at depths of >2000 ms TWT (ca. 2.3 km), the horizon is either difficult to interpret (discontinuous, low frequency and low amplitude) (Figure 7) or deeper than seismic record length.

The basin has a very thick Cenozoic fill, particularly in the northwest, where there are at least 4000 ms TWT (ca. 6.5 km) of Miocene-Recent sediments preserved (Figure 7a–c). In the seismic profiles to the southeast, the Miocene interval is significantly thinner (around 700 ms TWT [900 m]), and this is accompanied by minor thinning of the Plio-Pleistocene sequences, from around 1200 ms TWT (1200 m) thickness in the centre of the profile to around 800 ms TWT (700 m) of thickness in the southeast. Oligocene sequences are only mapped on the southwest, northeast and southeast flanks of the basin. Thickening and moderate structural uplift of the Oligocene sequences from southwest to northeast is observed from around 600 ms TWT (950 m) thickness near the N-1 well to 2000 ms TWT (3800 m) thickness near the DY-1 well (Figures 4 and 7e). Further southeast, significant uplift of the Oligocene sequences brings these close to the Plio-Pleistocene interval near the LD-1 well (Figures 4 and 7e).

The basin has an asymmetric shape (Figures 6 and 7). A series of basement-rooted, high-angle normal faults can be observed along the southwest margin, which downthrow the basement by up to 500 ms TWT (800 m) and extend up into the Pliocene sequences (Figure 7b,c,e). In the hangingwall of these faults, the Oligocene-Miocene sequences dip steeply into the basin, with the deepest part of the basin located <50 km away from this fault zone (Figures 5 and 6). By contrast, the northeast margin has a much gentler dip (Figure 7a–c).

The presence of discrete half-grabens within the basin can also be observed on these seismic profiles. These are defined by faults that affect mainly the Paleogene stratigraphy but that, in some instances, extend up into the Neogene or lowermost Pliocene stratigraphy (e.g. Figure 7e, point 1) with the greatest offsets at the top basement horizon. Evidence for structural inversion can also be found, including reverse faults that affect the Paleogene interval, folding of the Miocene interval and truncation beneath a prominent angular unconformity (Figure 7e, point 3).

4.2 | Paleogene rifting and transtension

The structural features of Paleogene half-grabens and grabens are demonstrated most clearly at the flanks of the basin (Figure 7d,e). The faults that define these grabens tip out mostly within the uppermost Oligocene/lowermost Miocene interval and cut down through to the basement. The exception to this is at the hinge zones where these large offset basement-rooted faults extend up through the entire Miocene interval into the Pliocene interval. However, the throw in the Miocene and Pliocene is relatively minor, suggesting that the displacement is due to variable compaction rather than continued tectonic extension.

There are limited areas where the features of the initial, late Eocene W-E rifts can be studied. In most regions, the rifts have been deeply buried and/or structurally inverted. However, there is one area on the northeast flank of the basin where these features are clearly preserved (Figures 7

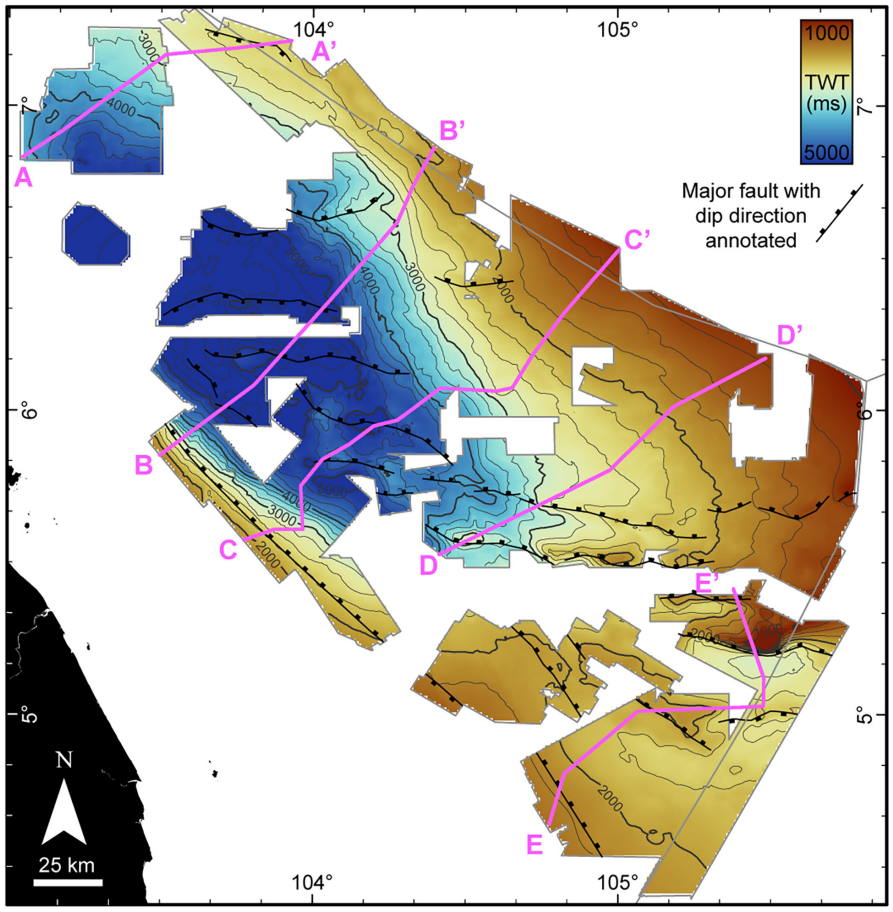

FIGURE 6 Intra-Group K time-structure map with some major fault zones annotated (after Tjia (1994)). The locations of seismic cross-sections shown in Figure 7 are also shown.

and 8). Here, a graben around 7–9 km wide and at least 50 km long is defined by two E–W-striking normal faults that downthrow the basement by >1200 m.

The internal seismic characteristics of the graben-fill are a thick package of tilted, faulted, and folded reflectors that are mostly discontinuous and low amplitude with some notably bright intervals (e.g. at the base). The fill is also highly structured. Some normal faulting can be observed, but there is also evidence of compression in the form of reverse faults, folding and reflector truncations (discussed in subsequent sections) (Figure 8). This graben lacks stratigraphic well control, however, it likely contains Eocene age (Groups L and older) continental clastic deposits observed in other parts of the basin.

There is also clear evidence from the seismic data of dextral fault movements, notably along the Western Hinge Fault Zone (Figure 9). In most instances, a NW-SE-striking deformation zone can be identified, but faults of varying geometry and size are also present (Figure 9). At the northwestern part of our dataset (Figure 9a,b), strike-slip characteristics are visible even at very shallow depths (Figure 9a). Here, long faults curve around from NW-SE to N–S (ca. 20° clockwise) with throws of up to 50 m. At deeper levels, long normal faults can also be observed (Figure 9b), but some antithetic and slightly oblique normal faulting creates small grabens with minor structural inversion.

In the SE of the basin, a cluster of small E–W fractures are oriented around 75° to two NW-SE-striking faults (Figure 9c). The orientation of these fractures suggests a link to the earlier Paleogene rifting phase within the basin. Further south, very distinct en-echelon fault geometries can be observed, consisting of multiple NNW–SSE Riedel shears and short SW–NE extensional faults (Figure 9d).

4.3 | Neogene inversion

The structural expression of two separate uplift events can be observed within the basin. The first event is tentatively dated as late Oligocene, and evidence is found on the flanks of the basin. In Figure 8, evidence for uplift (reverse faulting, folding) and erosion (truncation) can be observed towards the top of the syn-rift sequence, but the graben lacks biostratigraphic age constraints from wells to accurately date this event. The unconformity is probably equivalent to the late Oligocene unconformities observed in the West Natuna (Ginger et al., 1993) and Penyu (Madon et al., 2019) Basins. Several authors

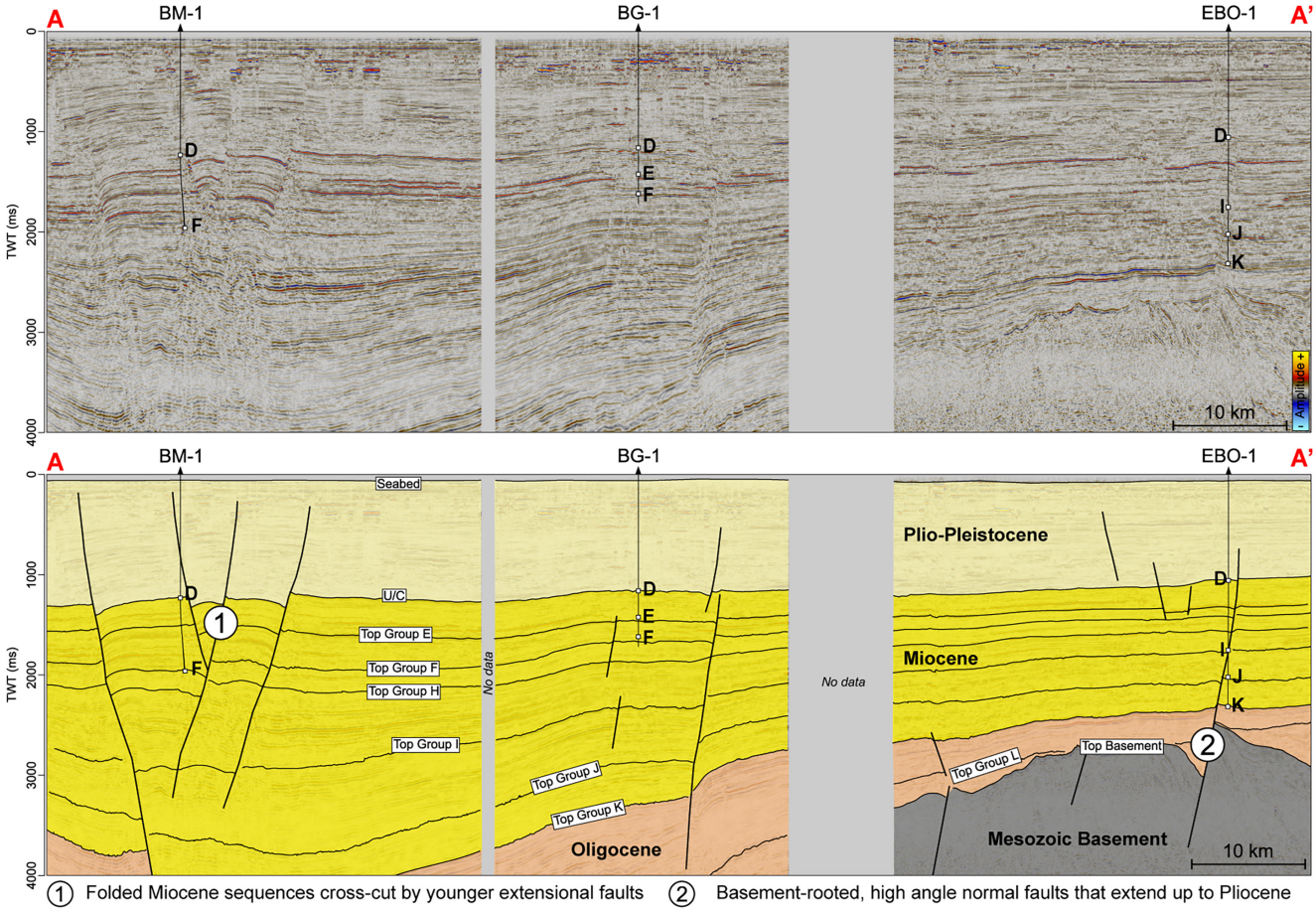

FIGURE 7 Un-interpreted (top) and interpreted (bottom) SW–NE-oriented regional seismic cross-sections (see Figures 4 and 6 for the location of the lines, labelled A-E). For simplicity, Group K to older is coloured as Oligocene in age, but Group K extends into the earliest Miocene (Figure 3).

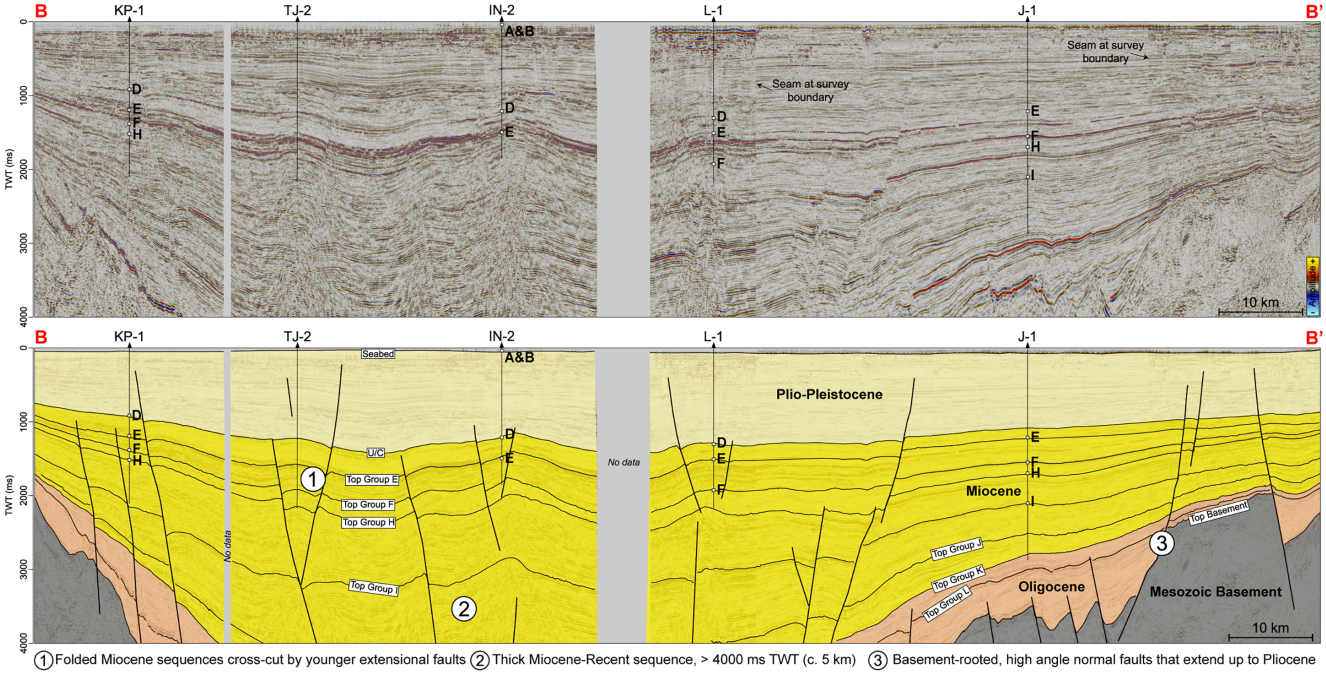

FIGURE 7 (Continued)

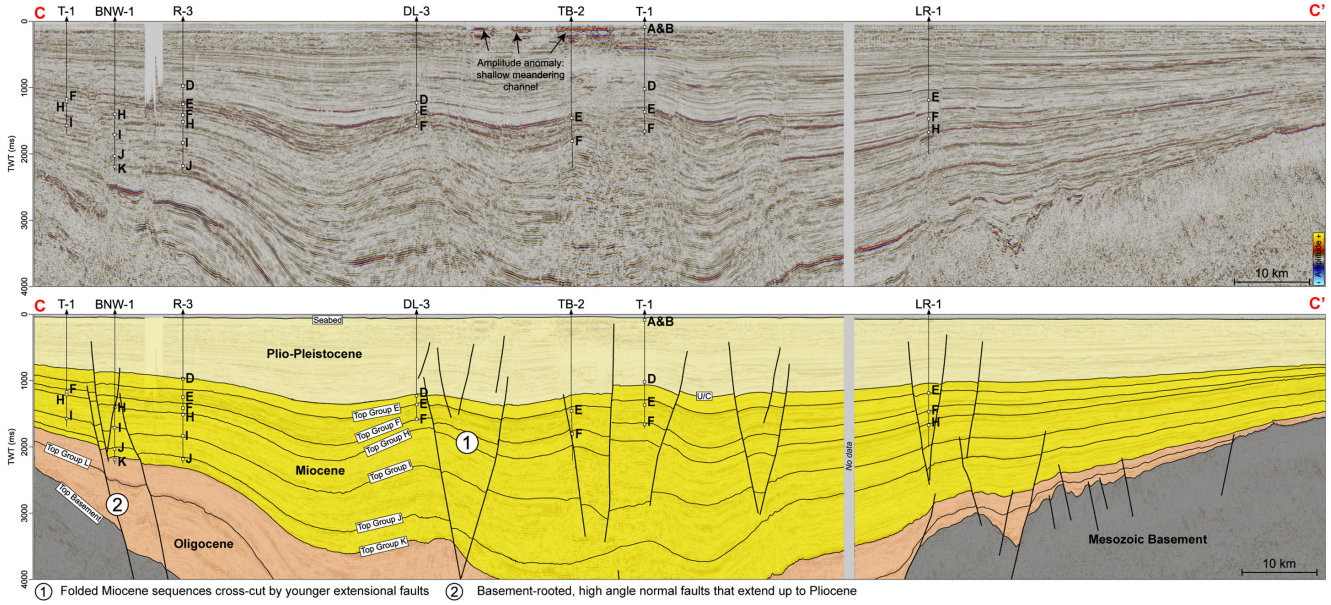

FIGURE 7 (Continued)

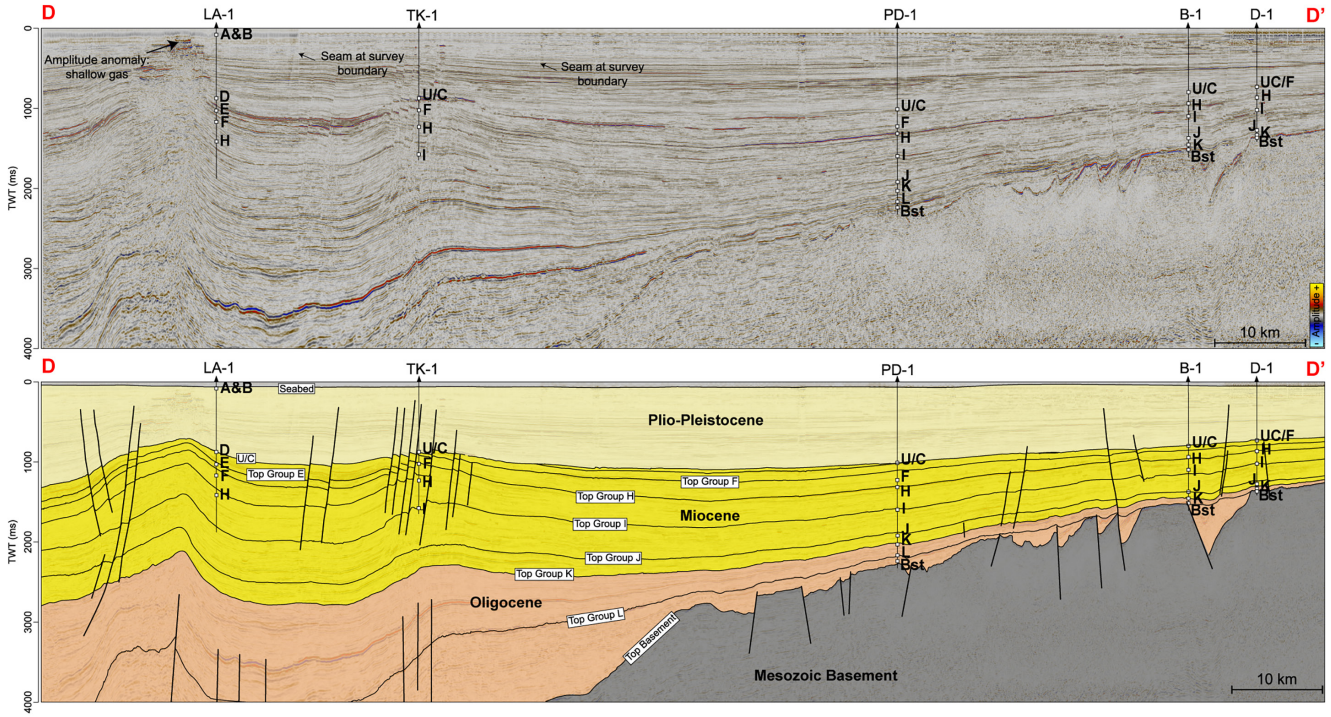

FIGURE 7 (Continued)

have attributed this uplift event to the onset of seafloor spreading of the South China Sea (Ginger et al., 1993; Morley, 2016; Morley et al., 2003).

The most prominent evidence for structural uplift is the folding of Miocene sequences and a large unconformity, the UMU. These folds form within a belt that runs through the centre of the basin (Figure 2), with their hinges striking W–E. They are associated with deeper W–E-striking faults (Figure 2), an example of which can be observed in the southwest part of Figure 7d beneath the LA-1 well. In this instance, a deeper reverse fault can be seen with the Miocene fold axis positioned above its hanging wall. This suggests that these folds were formed because of fault propagation, even though these faults are often too deeply buried in other parts of the basin to confirm this. There is little to inversion of the western

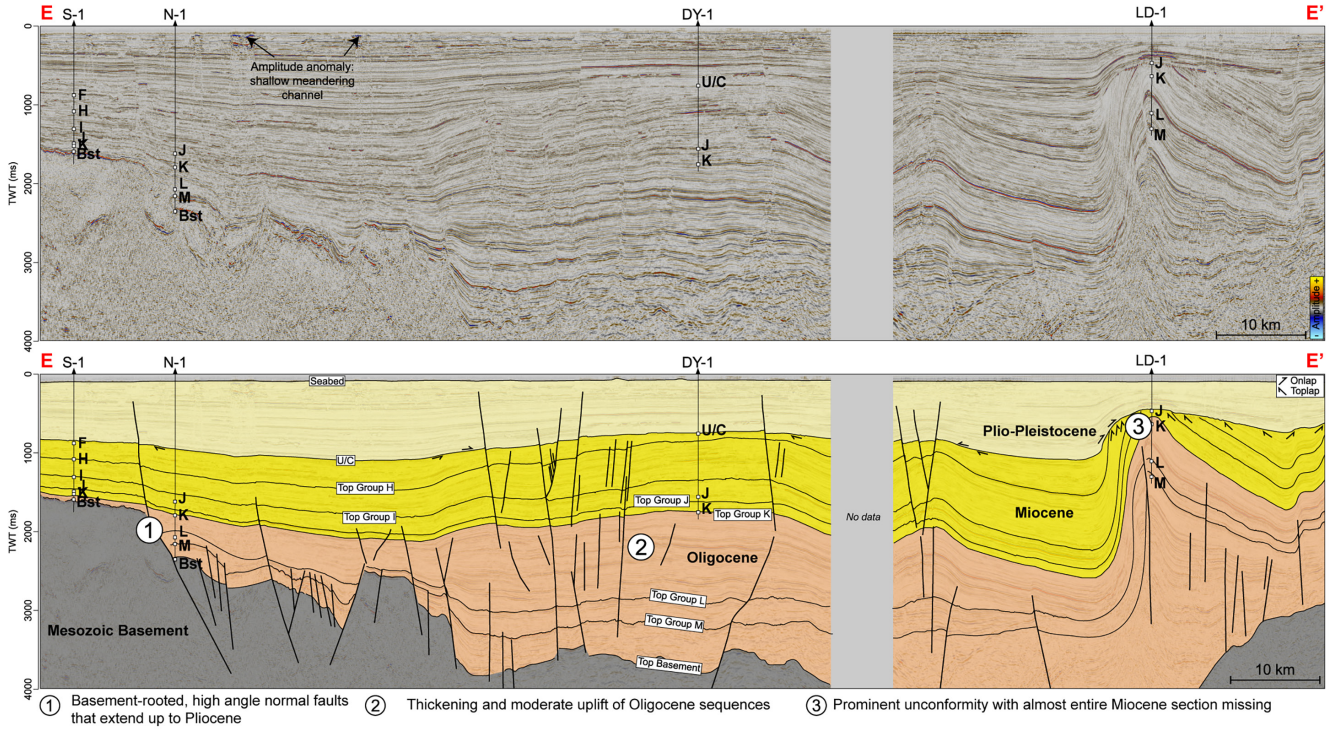

FIGURE 7 (Continued)

basement-rooted fault (Figure 7b,c,e) or faults along the eastern flank, with folding restricted to the central and deeper areas of the basin.

The folds are often crosscut by younger extensional faults that sole out mostly within the Miocene interval itself (Figure 7). The most dramatic evidence for compression and uplift is in the vicinity of the LD-1 well (Figure 4), where almost the entire Miocene interval has been removed, and there is a prominent angular unconformity separating the Plio-Pleistocene from the lowermost Neogene (Figure 7e). Towards the NE edge of this regional line, strong inversion and uplift around the L-1 well can be observed, with the UMU cutting down to intra-Group J. Looking in more detail at the area around the P-1 well (Figure 10), WNW-ESE-striking faults have experienced strong inversion with >60 m of reverse displacement at Group K level (Figure 10c). This produces large, WSW-ESE-striking anticlines with very steep limbs on the south side (Figure 10b). Small offset faults also affect the hangingwall, striking SW–NE, NW-SE and WSW-ENE. These faults appear to have retained normal displacement sense.

The UMU cuts through various intervals from the Miocene down to the upper Oligocene (Figure 3). To study this further, the subcrop to this unconformity was mapped using well penetrations and seismic mapping (Figure 11). Over much of the basin, the unconformity has only removed part of the Tortonian; Group D is preserved as a subcrop. In the east part of the basin, the unconformity is underlain by middle Miocene units (Groups F and H). This equates to a time gap of ca. 5–8 m.y. or a missing section of ca. 1500–2400 m, assuming 300 m per m.y. as a reasonable average post-rift sedimentation rate in the basin (Madon, 2007, Figure 12b).

The deepest erosion is limited to a small region in the SE, where the unconformity cuts down to Group K. This is a time gap of ca. 14 m.y., which could represent a missing section of up to 4200 m (following the same assumptions as stated above). This is significantly higher than previous estimates of the extent of uplift in this region (e.g. 1200 m; Du Bois, 1985).

In the central part of the basin, the UMU is less clear and separates Messinian Group A and B sediments from Tortonian sediments belonging to Group D (Figure 3). In these areas, the inversion of deeper grabens has generated anticlines, but no deep erosive event was observed in the southeast of the basin. In some areas (Figure 12a), Oligocene horizons can still be mapped with confidence. In addition, W-E-striking reverse faults can be observed, with anticlines developed within their hanging walls. These anticlines form along a set of ridges, a reflection of the original (now inverted) narrow rift system (Figure 2). In deeper areas of the basin, the syn-rift sequences are too deeply buried to be mapped, but anticlines can be mapped within the middle-upper Miocene stratigraphy (Figure 12b). Here, many of these anticlines are also crosscut by short, curved extensional faults.

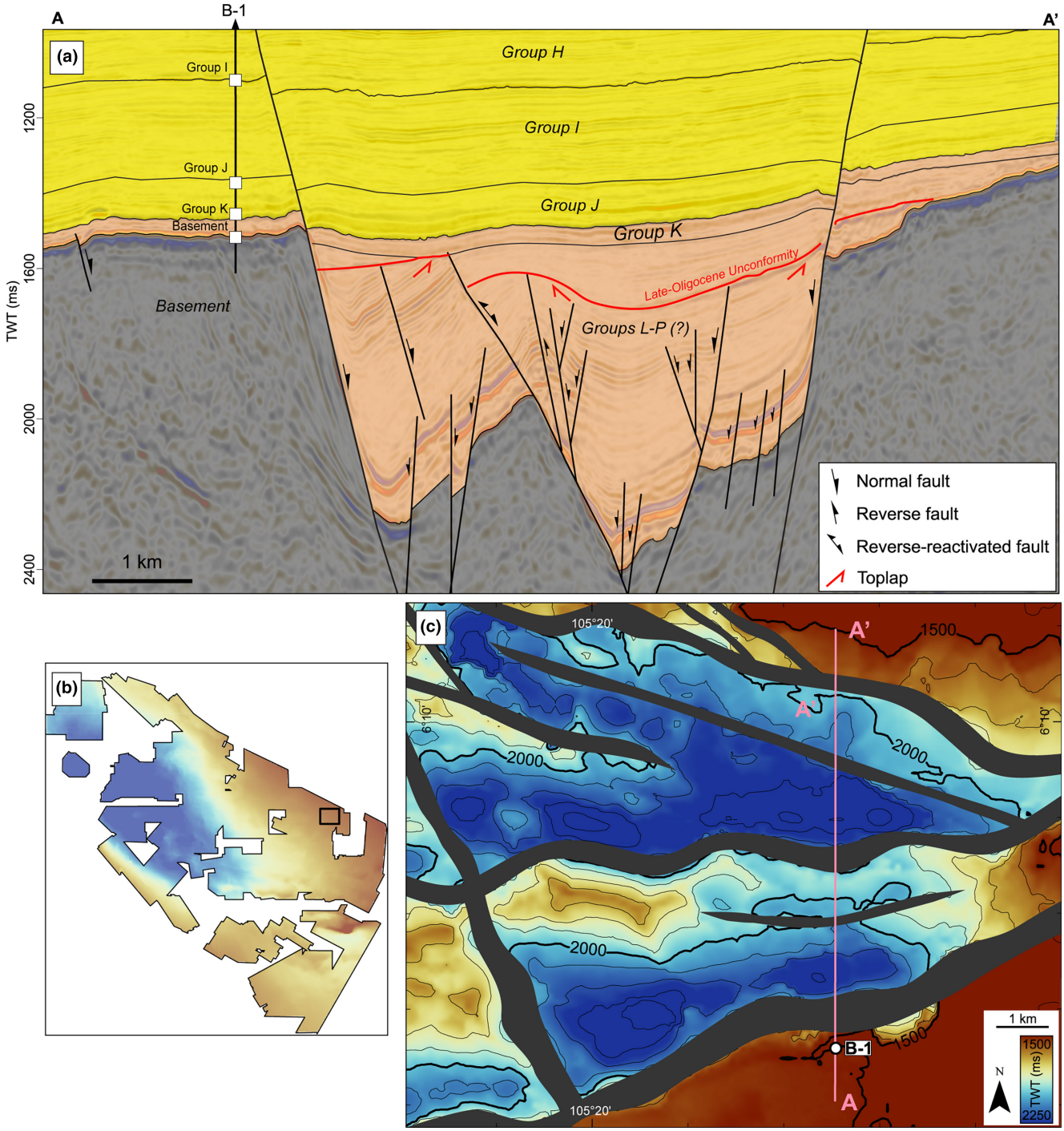

FIGURE 8 A series of illustrations highlighting the structure of a Paleogene graben north of the B-1 well. (a) S-N-oriented seismic cross-section highlighting the seismic characteristics of the graben-fill. (b) Regional location map showing the location of C. (c) Top structure map, in two-way-time (TWT), for the top basement horizon.

4.4 | Plio-Pleistocene characteristics

Evidence for tectonic quiescence during the Pliocene can be observed on a regional scale. Seismic horizons above the UMU dip gently across the basin, generally <1°, though there is some deformation above the E–W belt of anticlines (Figure 13a). This is in marked contrast to reflectors beneath the UMU, which show much more deformation, with the steepest dips (>10°) being associated with the Western Hinge Zone and the E–W anticlines (Figure 13b).

However, there are some subtle indications of structural events affecting the basin during this period. Some authors have noted a minor Intra-Pliocene

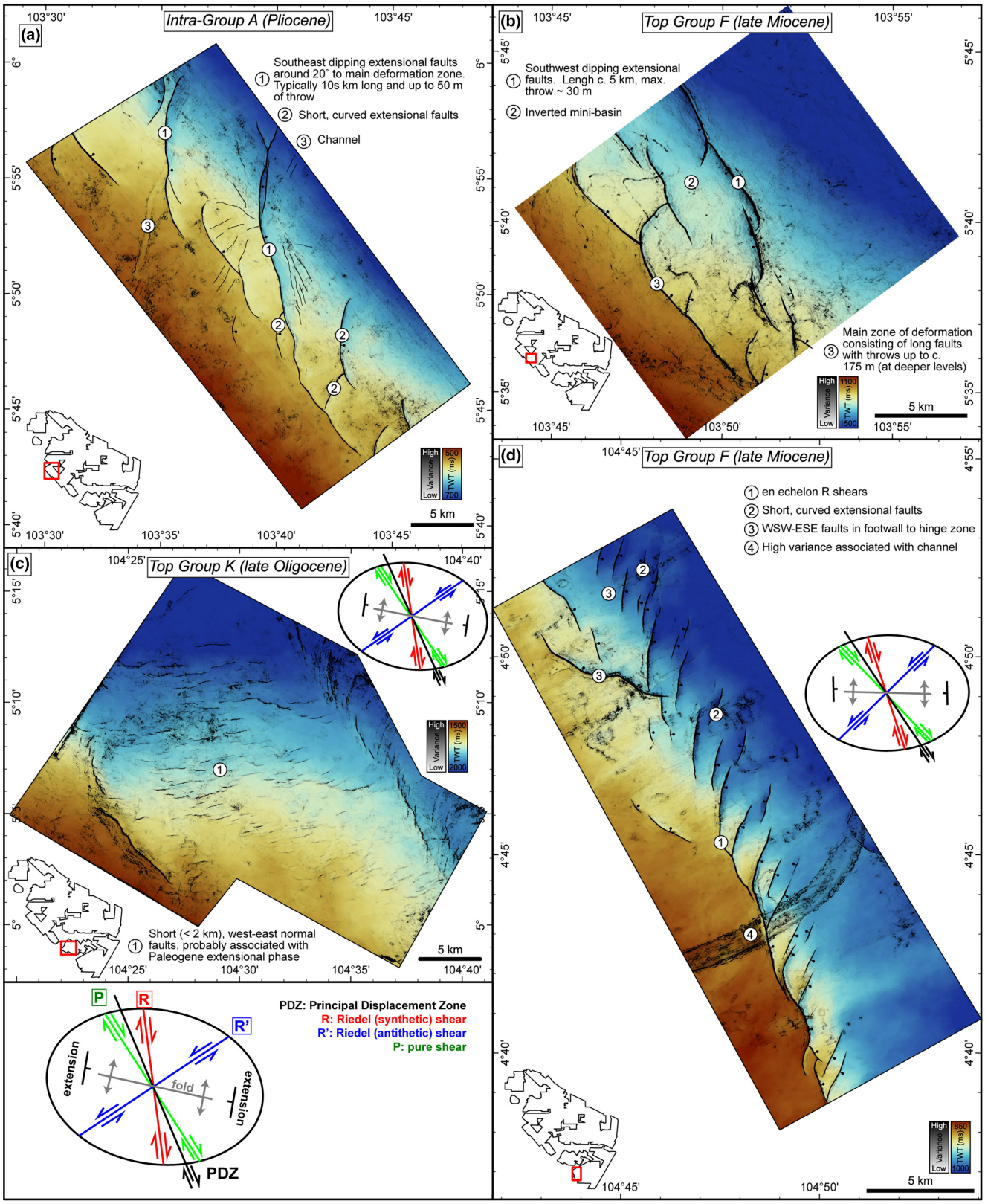

FIGURE 9 Top structure maps for four areas that illustrate strike-slip characteristics along the Western Hinge Fault Zone. (a) Intra-Group A (Pliocene), (b) Top Group F (late Miocene), (c) Top Group L (late Oligocene), (d) Top Group F (late Miocene). The red-to-blue colour bar represents the depth of the surface in two-way-time (TWT). The maps also contain a layer-blended seismic variance map for the corresponding horizon. Here, black colours indicate high seismic variance (low continuity—faults), and low seismic variance is transparent.

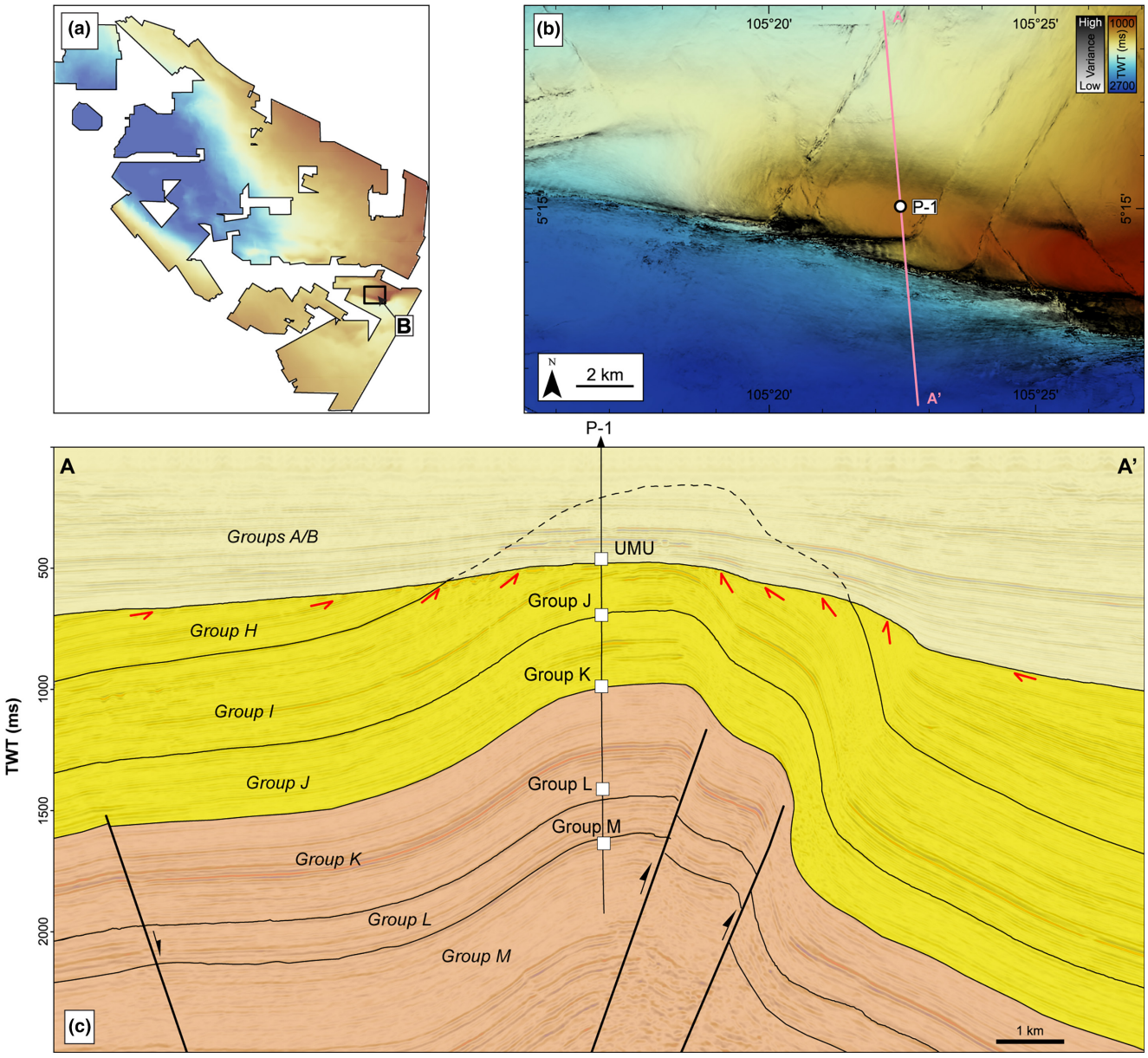

FIGURE 10 A series of illustrations highlighting the structure of the inverted region around the P-1 well. (a) Regional location map showing location of B, (b) Top structure map, in two-way-time (TWT), for a horizon within Group K, a layer-blended seismic variance map is also included (see caption in Figure 9 for description). (c) N-S-oriented seismic cross-section highlighting the truncation of Miocene reflectors beneath the Upper Miocene Unconformity (UMU).

unconformity (IPU) within wells located in the south-eastern Malay and West Natuna Basins (Armitage & Viotti, 1977; Lunt, 2021). One such well was Pulai-1 (Figure 4), in which Armitage and Viotti (1977) inferred the IPU based on the absence of palynological zone N20 (ca. 3 Ma) within the Pilong Formation (Group A and B) (Figure 3), and a high amplitude seismic reflector around the well (Figure 14). This seismic reflector is at 475 ms TWT (385 m MD in the well), some 100 ms TWT shallower than the UMU (around 580 ms TWT or 478 m MD in the well, Figure 14). Lunt (2021) discussed that the IPU could result from a regional drop in base level associated with stronger glacio-eustatic control during the mid-Pliocene. An upward decrease in the gamma-ray log within the interval beneath the IPU at Pulai-1 (Figure 14) could be interpreted as a regressive event, aligning with other authors' observations of a shallowing in depositional facies up through the Pliocene (e.g. West Natuna Basin: Darmadi et al., 2007 and Nam Con Son Basin: Matthews et al., 1997).

There is also evidence of structural deformation in the deeper part of the basin to the north. Previous

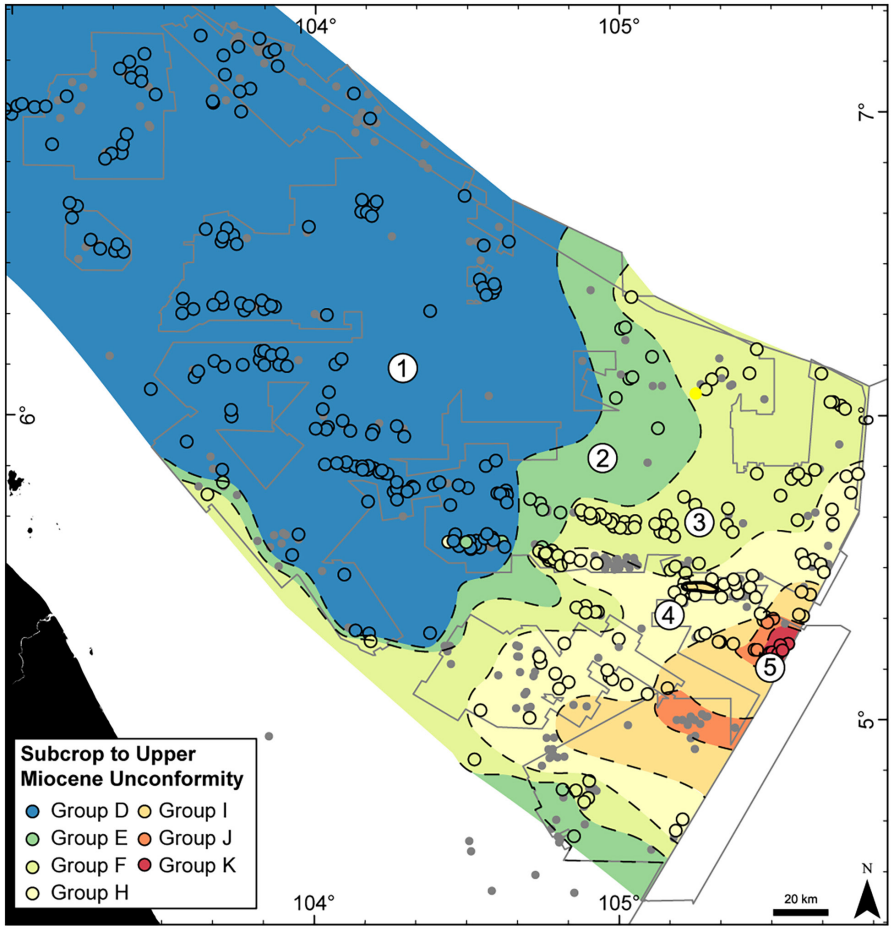

FIGURE 11 1: 0.5 m.y. time gap, ca. 150 m missing section, 2: 1.5–5 m.y. time gap, ca. 450–1500 m missing section, 3: 5–7.5 m.y. time gap, ca. 1500–2250 m missing section, 4: 7.5–9.5 m.y. time gap, ca. 2250–2850 m missing section, 5: Up to 17 m.y. time gap, up to ca. 5 km missing section.

authors have noted an N–S-striking fault zone that particularly affects the central and western parts of the basin (Liew, 1997; Tjia, 1994). This zone has been used to broadly separate the Malay Basin into a northern domain consisting of N–S-striking faults and a southern domain consisting of E–W-striking faults (Figure 2; Liew, 1997; Tjia & Liew, 1996). The structural characteristics of this area can be observed from a top structure map of the UMU in the northwest of the basin (Figure 15), which lies within the N-S-striking Kapal-Bergading and Kuda-Ular fault zones (Tjia & Liew, 1996). Here, many long (10–20 km) curvilinear faults with throws up to ca. 200 m crosscut the UMU with orientations around N–S to NNE–SSW (Figure 15). It is difficult to ascertain if these faults extend down to the basement due to its burial depth, but the faults appear to cut through most of the Oligocene–Miocene fill and previous authors have suggested these fault zones formed following the reactivation of N–S basement faults akin to those onshore Peninsular Malaysia (Liew, 1994, 1997). Some shorter (mainly <5 km) faults also affect anticlines within the centre of the basin (e.g. Figure 12). These have previously been attributed to crestal collapse following the late Miocene compressional events (Tjia, 1994).

During this period of steady subsidence, accommodation space within the Malay Basin was quickly filled. It is suggested that by the late Pliocene, fluvial systems bypassed the basin entirely and instead flowed south and east towards the Nam Con Son Basin and the South China Sea (Murray & Dorobek, 2004). However, as noted above, a significant sea level drop occurred within the Pliocene, leading to the resumption of fluvial deposition in the Malay Basin. Global cooling during the Plio-Pleistocene led to a gradual drop in global sea levels, and the Sunda Shelf was permanently exposed at around 400 ka (Sarr et al., 2019). However, continued subsidence of the shelf, combined with oscillations in sea level, resulted in the shelf experiencing intermittent periods of submersion and exposure after 400 ka (McGrath et al., 2023; Sarr et al., 2019).

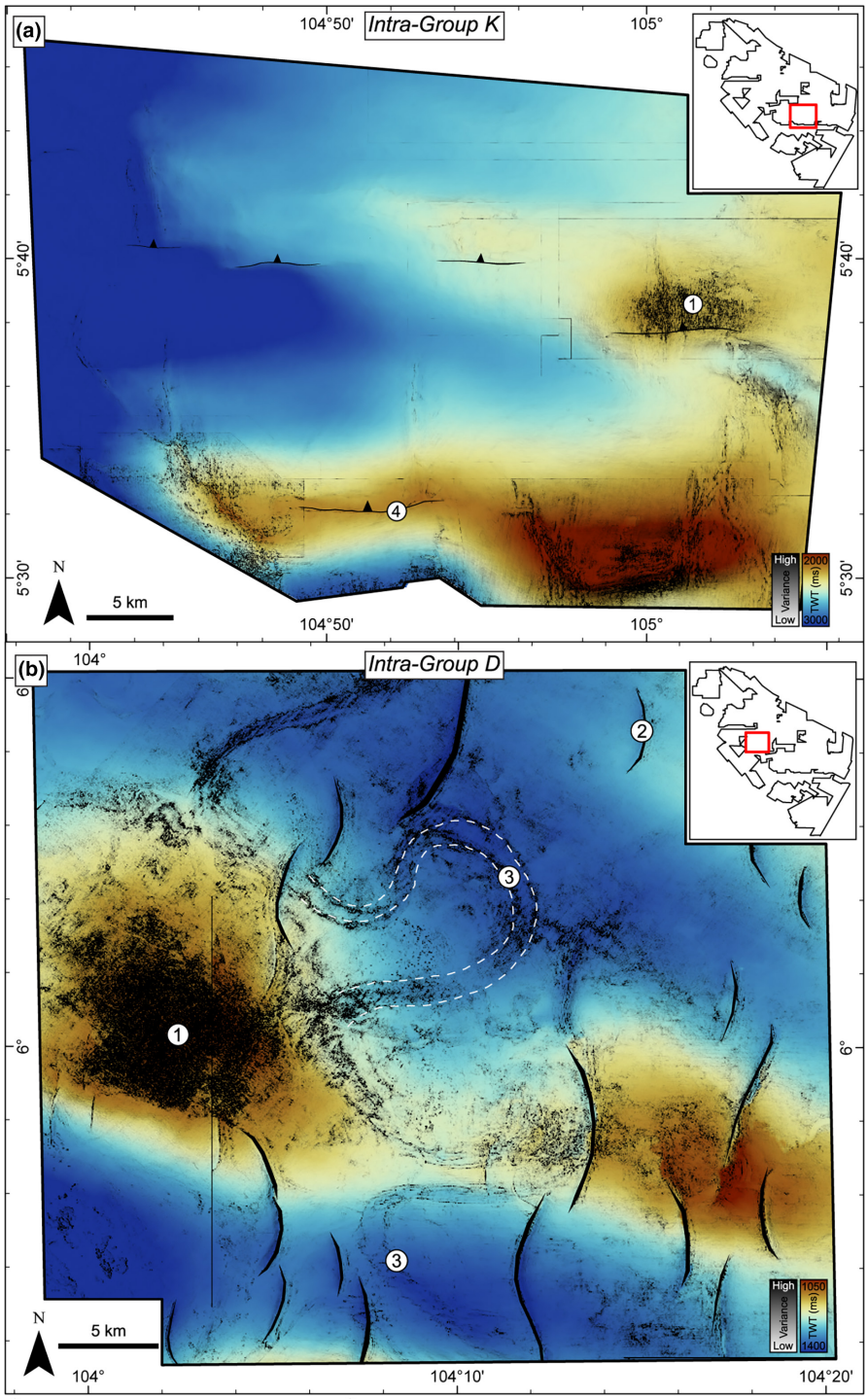

FIGURE 12 Top structure maps showing anticlines in two central areas of the basin ((a) Intra-Group K, (b) Intra-Group D). The red-to-blue colour bar represents the depth of the surface in two-way-time (TWT). The maps also contain a layer-blended seismic variance map for the corresponding horizon to highlight faults or other seismic discontinuities such as gas clouds.

4.5 | Trap analysis and implications for CCS

Following the development of a structural and stratigraphic framework for the basin, we re-evaluated the main trapping mechanisms within existing hydrocarbon fields. The rationale for this is to constrain which trap types might be better suited to CO_2 storage (i.e. those with high capacity and low containment risk) and how these are distributed across the basin.

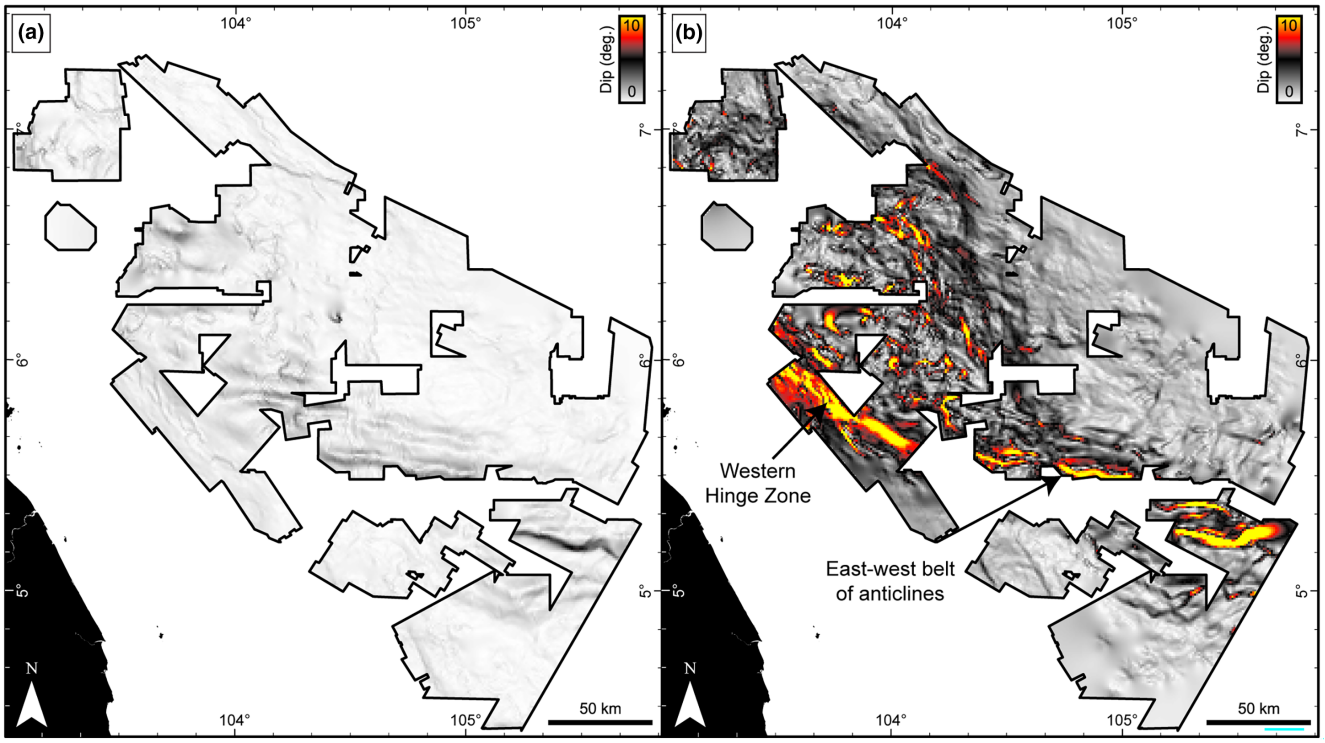

FIGURE 13 Dip maps for an intra-Pliocene horizon (a) and intra-Oligocene horizon (b) with identical colour scaling.

To achieve this, the main trapping mechanism for ca. 200 hydrocarbon discoveries was analysed systematically by integrating the results of our mapping with descriptions from well reports and previous studies where available. A scheme modified slightly from Vincelette et al. (1999) was adopted, which led us to classify 11 different trap types (Figure 16a,b). Around one-third of traps developed within folds associated with the inversion of deeper fault zones (Figure 16b). These traps consist of several stacked reservoir horizons folded into a four-way dip closure (Figure 16e), forming some of the largest oil and gas discoveries in the basin (Madon, 2021). They form a belt that runs E–W from the maritime border with Indonesia towards the centre of the basin where it bends upwards to run parallel with the shoreline of Peninsular Malaysia (Figure 16a). Most of these folds are oriented E–W (28%), but some are also oriented NW-SE and SW–NE, located mainly to the south and southeast areas of the basin, respectively.

While the largest structural traps in a basin may be obvious targets for CO_2 storage, the presence of shallow gas above many of these anticlines must be seen as a significant risk for storage containment that requires further analysis. Intervals of high seismic variance, high noise, and low reflector continuity overly these anticlines (Figure 12b) which strongly implies breach of these structural traps. At the moment, it is not clear what the rate of leakage is (and if this is of concern for storage or not) or if the leakage mechanisms are via small faults or existing/induced fractures, or by advection through the caprock matrix when overcoming the capillary entry pressure.

Fault-associated traps are the other dominant trapping mechanism in the basin, accounting for ca. 45% of our analysed discoveries (Figure 16b). Here, we include anticlines developed within the hangingwall of extensional faults (rollover anticlines) and tilted fault blocks that rely on some element of fault seal either across the hangingwall or the footwall (Figure 16d). In the case of the former, these are more prevalent in the north and northwest of the basin, where they are often associated with N-S-striking faults such as the Kuda-Ular fault zone (see Section 4.4). In some cases, a single fault will have a rollover anticlinal trap and a footwall tilted fault block trap associated with it, as shown by the pairing of each trap type in the northwest of the basin (Figure 16a,d). Tilted fault block traps in the Malay Basin are usually fairly small, and this, combined with the requirement for a lateral fault seal, probably makes them less attractive targets for CO_2 storage. Determining fault seal efficacy would require analysis of geometry, juxtaposition and host rock properties on either side of the fault, and the presence of hydrocarbon accumulations within shallow intervals associated with these faults is evidence that fluid flow up some faults in the basin is possible. While rollover anticlines are by definition associated with a fault, the closures are often purely formed by structural dip and are thus lower risk traps.

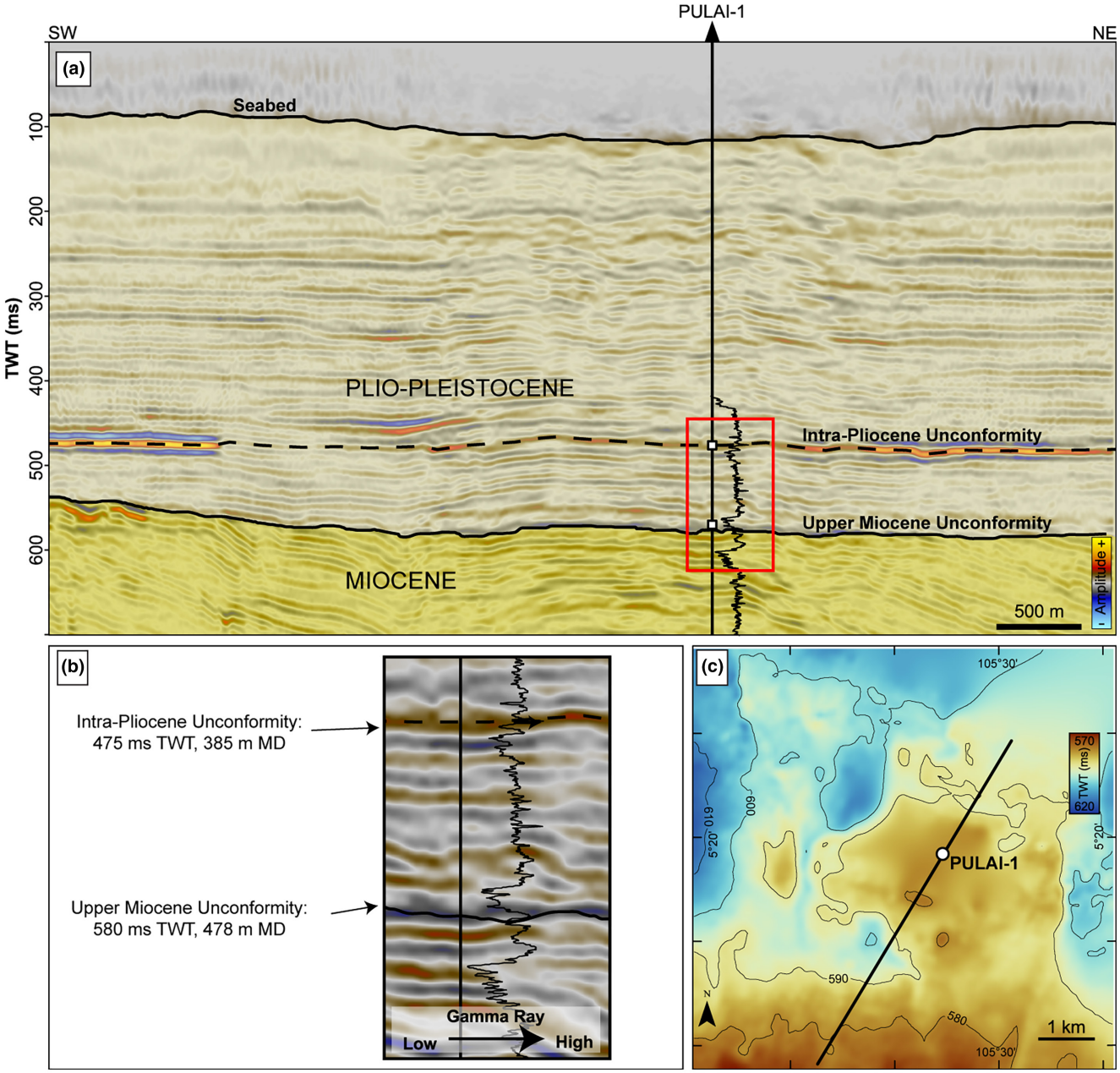

FIGURE 14 (a) Southwest-northeast oriented cross-section through PULAI-1 well. (b) Expanded view of gamma ray log highlighting two unconformities. (c) Map showing location of cross-section and well. The well is in the southeast of the basin, please refer to Figure 4.

Traps that relate to a basement high are preferentially located at the edges of the basin (Figure 16a). These include those formed by a structural drape of sediments over a basement high. These traps are mostly low-relief and mainly constrained to the Oligocene- lower Miocene horizons (Figure 16c). These traps do not show the same evidence for fluid leakage as the large anticlinal traps, but on the other hand, are much smaller in size. Fractured basements and traps with an up-dip seal against a basement high are only documented in a few cases and are unlikely to be serious targets for CO_2 storage in lieu of lower-risk locations. Such traps are only documented in a few cases and structural drape is the dominant mechanism (12% of our total analysed discoveries).

Structural trapping is an important mechanism for CO_2 storage within aquifer systems. Upon injection into an aquifer, the CO_2 plume will migrate up-dip, filling any structural traps successively in a concept often referred to as a "trapping chain" (de Jonge-Anderson et al., 2024). Each structure will have its own associated risk of leakage. For example, large fold traps in the Malay Basin are often associated with seismic features indicative of shallow gas and leakage from the reservoir. Fault-seals can also bring inherent risks that need to be analysed on a case-by-case basis, accounting for fault geometry and rock properties to assess their leakage

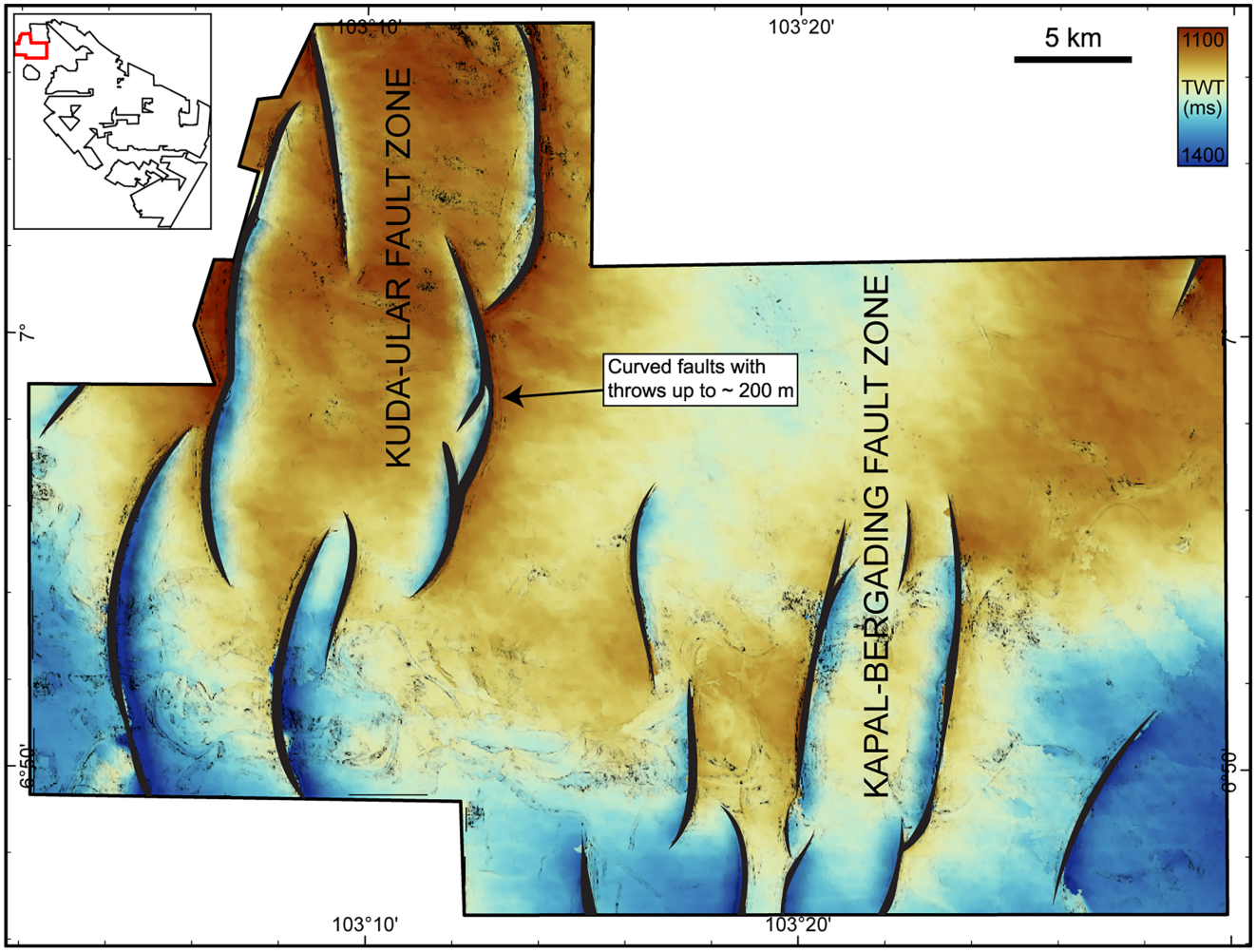

FIGURE 15 Top structure map for an area in the northwest of the basin. The red-to-blue colourbar represents the depth of the surface in two-way-time (TWT). The maps also contain a layer-blended seismic variance map for the corresponding horizon to highlight faults and other seismic discontinuities.

potentials. By identifying the domains shown in Figure 16, we provide an initial indication of the trapping styles expected within certain parts of the basin, and a concept that can be tested with subsequent plume migration simulations.

5 | CONCLUSIONS

Using newly available, regional, 3D seismic and well data for the Malay Basin, we present a detailed analysis of the structural and stratigraphic evolution of the basin and consider implications for CO_2 storage potential.

Rifting started occurring during the late Eocene when sinistral motion across NW-SE-striking strike-slip faults produced W-E-striking faults and narrow sub-basins. These basins were filled with Eocene–Oligocene continental clastic sediments before a late Oligocene compressional event uplifted and folded these sequences to produce an angular unconformity. More widespread opening of the basin started during the late Oligocene when dextral motion across NW-SE-striking strike-slip zones generated N–S-striking en-echelon faults and ridges. Strike-slip deformation is evident along the Western Hinge Zone and consists of en-echelon faults, oblique shear faults and perpendicular tensional fractures. Following a tectonically quiescent post-rift phase, two prominent unconformities are present during the middle-late Miocene. An MMU has removed parts of Group E and is likely linked to sea-level fall associated with the emergence of the Natuna area to the southeast. Inversion occurred throughout the late Miocene, culminating in a regional unconformity with up to 4.2 km of Miocene sediments eroded in the SE of the basin. There was little tectonic activity during the Pliocene–Pleistocene, but some faulting affects the northwest of the basin, and there is some evidence of an IPU generated by regional sea-level fall.

These new structural and stratigraphic observations allow us to delineate several trapping domains across the basin. These trapping domains help us to identify areas

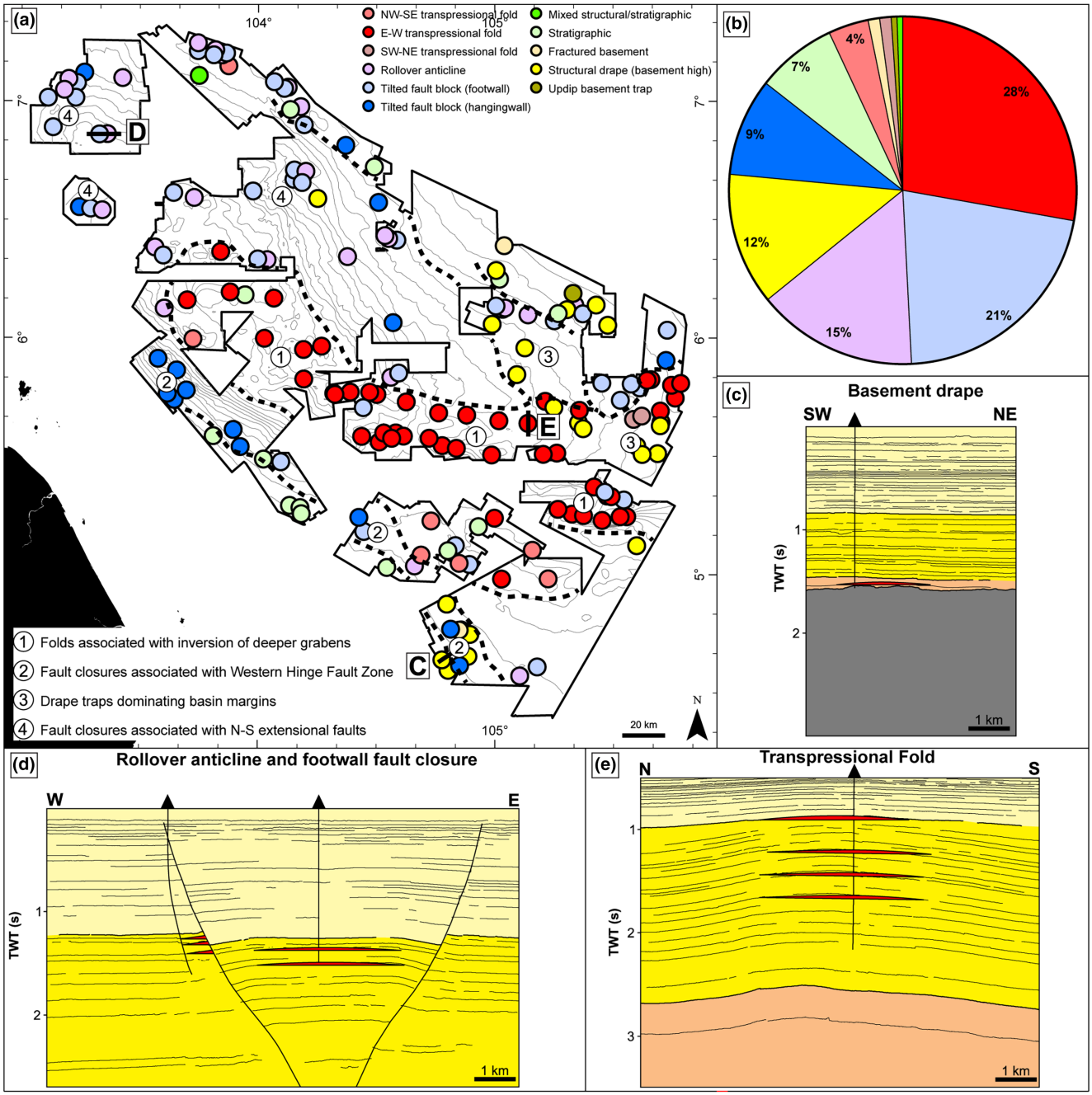

FIGURE 16 Classification of ca. 200 discoveries by trap type shown in map view (a) and as a pie chart (b). Examples of the main trap types are also shown in the form of structural cross-sections from seismic data (c–e). Base contours in (a) are taken from Figure 6 (intra-Group K horizon).

where additional structural closures may exist within saline aquifers that could be targeted for CO_2 storage. Future work should involve a more detailed analysis of trapping styles and seal efficacy to de-risk potential containment issues associated with shallow gas.

ACKNOWLEDGEMENTS

SLB and ESRI are thanked for providing academic licences for Petrel and ArcGIS Pro, both of which facilitated this work. Gerome Calves, Peter Clift and Kara English are thanked for their thorough and constructive reviews of this manuscript.

FUNDING INFORMATION

The funding and data underpinning this work was provided by PETRONAS via the PETRONAS Centre of Excellence in Subsurface Engineering and Energy Transition (PACESET), based at Heriot-Watt University.

PEER REVIEW

The peer review history for this article is available at https://www.webofscience.com/api/gateway/wos/peer-review/10.1111/bre.12885.

DATA AVAILABILITY STATEMENT

Research data are not shared.

ORCID

Iain de Jonge-Anderson https://orcid.org/0000-0002-9438-8194
Andreas Busch https://orcid.org/0000-0002-3279-5202
Florian Doster https://orcid.org/0000-0001-7460-573X
Uisdean Nicholson https://orcid.org/0000-0003-0746-8549

REFERENCES

Abd Rahman, I. Z., Abang Hasbollah, D. Z., Mohd Yunus, N. Z., Kasiman, E. H., & Mazlan, A. N. (2022). Carbon dioxide storage potential in Malaysian sandstone aquifer: An overview. *IOP Conference Series: Earth and Environmental Science*, *971*(1), 012022. https://doi.org/10.1088/1755-1315/971/1/012022

Ahmed Satti, I., Wan Yusoff, W. I., & Ghosh, D. (2016). Overpressure in the Malay Basin and prediction methods. *Geofluids*, *16*(2), 301–313. https://doi.org/10.1111/gfl.12149

Almasgari, A. A., Elsaadany, M., Latiff, A. H. A., Hermana, M., Rahman, A. H. B. A., Babikir, I., Imran, Q. S., Appiah, N. F., & Adeleke, T. O. (2020). Application of seismic attributes to delineate the geological features of the Malay Basin. *Bulletin. Geological Society of Malaysia*, *69*, 97–110. https://doi.org/10.7186/bgsm69202009

Alqahtani, F. A., Jackson, C. A.-L., Johnson, H. D., & Som, M. R. B. (2017). Controls on the geometry and evolution of humid-tropical fluvial systems: Insights from 3D seismic geomorphological analysis of the Malay Basin, Sunda Shelf, Southeast Asia. *Journal of Sedimentary Research*, *87*(1), 17–40. https://doi.org/10.2110/jsr.2016.88

Alqahtani, F. A., Johnson, H. D., Jackson, C.A.-L., & Som, M. R. B. (2015). Nature, origin and evolution of a Late Pleistocene incised valley-fill, Sunda Shelf, Southeast Aasia. *Sedimentology*, *62*(4), 1198–1232. https://doi.org/10.1111/sed.12185

Argus, D. F., Gordon, R. G., & DeMets, C. (2011). Geologically current motion of 56 plates relative to the no-net-rotation reference frame: NNR-MORVEL56. *Geochemistry, Geophysics, Geosystems*, *12*(11). 1–13. https://doi.org/10.1029/2011GC003751

Armitage, J. H., & Viotti, C. (1977). Stratigraphic nomenclature-southern end Malay Basin. Proceedings of the Indonesian Petroleum Association, 6th Annual Convention https://doi.org/10.29118/IPA.1281.69.94

Arshad, A. R. M., Mhd, D., & Tjia, H. D. (1995). A deep seismic section across the Malay Basin: Processing of data and tectonic interpretation. *Warta Geologi (Newsletter of the Geological Society of Malaysia)*, *21*(6), 412.

Babikir, I., Salim, A. M. A., Hermana, M., Abdul Latiff, A. H., & Al-Masgari, A. A.-S. (2022). Characterizing the subsea Pleistocene fluvial system of the Sunda shelf, offshore Malaysia, using multiattribute corendering and self-organizing maps. *Interpretation*, *10*(2), T291–T304. https://doi.org/10.1190/INT-2021-0005.1

Bird, P. (2003). An updated digital model of plate boundaries. *Geochemistry, Geophysics, Geosystems*, *4*(3), 2001GC000252. https://doi.org/10.1029/2001GC000252

Bishop, M. (2002). Petroleum systems of the Malay Basin Province, Malaysia. Open-File Report, U.S. Geological Survey, 99-50.

Bustin, R. M., & Chonchawalit, A. (1995). Formation and tectonic evolution of the Pattani Basin, gulf of Thailand. *International Geology Review*, *37*(10), 866–892. https://doi.org/10.1080/00206819509465431

Clift, P., Lee, G. H., Anh Duc, N., Barckhausen, U., Van Long, H., & Zhen, S. (2008). Seismic reflection evidence for a dangerous grounds miniplate: No extrusion origin for the South China Sea. *Tectonics*, *27*(3), 2007TC002216. https://doi.org/10.1029/2007TC002216

Darmadi, Y., Willis, B. J., & Dorobek, S. L. (2007). Three-dimensional seismic architecture of fluvial sequences on the low-gradient Sunda shelf, offshore Indonesia. *Journal of Sedimentary Research*, *77*(3), 225–238. https://doi.org/10.2110/jsr.2007.024

Doust, H. (2017). Petroleum systems in Southeast Asian Tertiary basins. *Bulletin. Geological Society of Malaysia*, *64*(1), 1–16. https://doi.org/10.7186/bgsm64201701

Doust, H., & Sumner, H. S. (2007). Petroleum systems in rift basins—A collective approach in Southeast Asian basins. *Petroleum Geoscience*, *13*(2), 127–144. https://doi.org/10.1144/1354-079307-746

Du Bois, E. P. (1985). Review of principal hydrocarbon-bearing basins around the South China Sea. *Bulletin. Geological Society of Malaysia*, *18*, 167–209. https://doi.org/10.7186/bgsm18198508

Fyhn, M. B. W., Boldreel, L. O., & Nielsen, L. H. (2010). Escape tectonism in the Gulf of Thailand: Paleogene left-lateral pull-apart rifting in the Vietnamese part of the Malay Basin. *Tectonophysics*, *483*(3–4), 365–376. https://doi.org/10.1016/j.tecto.2009.11.004

GEBCO Compilation Group. (2023). GEBCO 2023 grid. https://doi.org/10.5285/F98B053B-0CBC-6C23-E053-6C86ABC0AF7B

Ginger, D. C., Ardjakusumah, W. O., Hedley, R. J., & Pothecary, J. (1993). Inversion history of the West Natuna Basin: Examples from the Cumi-Cumi PSC. Proceedings Indonesian Petroleum Association: 22nd Annual Convention, 635–658.

Hall, R., Clements, B., & Smyth, H. R. (2009). Sundaland: Basement character, structure and plate tectonic development. Proceedings of the Indonesian Petroleum Association, thirty-third annual convention https://doi.org/10.29118/IPA.2374.09.G.134

Hall, R., & Morley, C. K. (2004). Sundaland basins. In P. Clift, W. Kuhnt, P. Wang, & D. Hayes (Eds.), *Geophysical monograph series* (Vol. *149*, pp. 55–85). American Geophysical Union. https://doi.org/10.1029/149GM04

Hasbollah, D. Z. A., Junin, R., Taib, A. M., & Mazlan, A. N. (2020). Basin evaluation of CO_2 geological storage potential in Malay Basin, Malaysia. In P. Duc Long & N. T. Dung (Eds.), *Geotechnics for sustainable infrastructure development* (Vol. *62*, pp. 1405–1410). Springer. https://doi.org/10.1007/978-981-15-2184-3_184

Heflin, M., Donnellan, A., Parker, J., Lyzenga, G., Moore, A., Ludwig, L. G., Rundle, J., Wang, J., & Pierce, M. (2020). Automated

estimation and tools to extract positions, velocities, breaks, and seasonal terms from daily GNSS measurements: Illuminating nonlinear salton trough deformation. Earth and space. *Science*, *7*(7), e2019EA000644. https://doi.org/10.1029/2019EA000644

Hou, J., Takahashi, T., Katoh, A., Jaroonsitha, S., Chumsena, K. P., & Nakayama, K. (2008). Application of seismic attributes and neural network for sand probability prediction—A case study in the North Malay Basin. *Bulletin. Geological Society of Malaysia*, *54*, 115–121. https://doi.org/10.7186/bgsm54200818

Hutchison, C. S. (2005). *Geology of North-West Borneo: Sarawak, Brunei and Sabah* (1st ed.). Elsevier.

Hutchison, C. S., Bergman, S. C., Swauger, D. A., & Graves, J. E. (2000). A Miocene collisional belt in north Borneo: Uplift mechanism and isostatic adjustment quantified by thermochronology. *Journal of the Geological Society*, *157*(4), 783–793. https://doi.org/10.1144/jgs.157.4.783

Jirin, S., Mohamed, M., & Hasan, S. S. (2013). Transgressive-regressive cycles in the Malay Basin: New insights. IPTC https://doi.org/10.2523/IPTC-16838-Abstract

de Jonge-Anderson, I., Ramachandran, H., Nicholson, U., Geiger, S., Widyanita, A., & Doster, F. (2024). Determining CO2 storage efficiency within a saline aquifer using reduced complexity models. *Advances in Geo-Energy Research*, *13*(1), 22–31.

Jumari, N. I., Mohaman, H., & Ahman, N. (2011). Seismic facies analysis of group L and M reservoirs southeast of Malay Basin. *Warta Geologi (Newsletter of the Geological Society of Malaysia)*, *37*(1), 55.

Kessler, F. L., Jong, J., & Madon, M. (2021). Sedimentary record of Paleogene sequences in the Penyu and Malay basins, offshore peninsular Malaysia. *Berita Sedimentologi*, *46*(1), 6–20. https://doi.org/10.51835/bsed.2020.46.1.57

Kuang, K. S. (1988). Structural history of the Malay Basin, a classical tertiary wrench basin. *Warta Geologi (Newsletter of the Geological Society of Malaysia)*, *14*(6), 263.

Liew, K. K. (1994). Structural development at the west-central margin of the Malay Basin. *Bulletin. Geological Society of Malaysia*, *36*, 67–80.

Liew, K. K. (1997). Structural analysis of the Malay Basin. *Bulletin. Geological Society of Malaysia*, *40*, 157–176. https://doi.org/10.7186/bgsm40199712

Lunt, P. (2021). A reappraisal of the Cenozoic stratigraphy of the Malay and West Natuna basins. *Journal of Asian Earth Sciences*, *5*, 100044. https://doi.org/10.1016/j.jaesx.2020.100044

Madon, M. (1994). Depositional and diagenetic histories of reservoir sandstones in the Jerneh field, central Malay Basin. *Bulletin. Geological Society of Malaysia*, *36*, 31–53.

Madon, M. (1997). The kinematics of extension and inversion in the Malay Basin, offshore peninsular Malaysia. *Bulletin. Geological Society of Malaysia*, *41*, 127–138. https://doi.org/10.7186/bgsm41199711

Madon, M. (2007). Overpressure development in rift basins: An example from the Malay Basin, offshore peninsular Malaysia. *Petroleum Geoscience*, *13*(2), 169–180. https://doi.org/10.1144/1354-079307-744

Madon, M. (2011). Transgressive-regressive cycles in the Malay Basin: The interplay of tectonics and sea level changes in a Silled Basin. *PGCE*, *2011*, 76–77. https://doi.org/10.3997/2214-4609-pdb.251.49

Madon, M. (2021). Five decades of petroleum exploration and discovery in the Malay Basin (1968-2018) and remaining potential. *Bulletin. Geological Society of Malaysia*, *72*, 63–88. https://doi.org/10.7186/bgsm72202106

Madon, M., Abolins, P., Hoesni, M. J., & Ahmad, B. (1999). Malay Basin. In *The petroleum geology and resources of Malaysia* (pp. 173–217). Petronas.

Madon, M., Jong, J., Kessler, F. L., Damanhuri, M. H., & Amin, M. K. A. (2020). Pre-tertiary basement subcrops beneath the Malay and Penyu basins, offshore peninsular Malaysia: Their recognition and hydrocarbon potential. *Bulletin. Geological Society of Malaysia*, *70*(1), 163–193. https://doi.org/10.7186/bgsm70202014

Madon, M., Jong, J., Kessler, F. L., Murphy, C., Your, L., Hamid, A. M., & Sharef, N. (2019). Overview of the structural framework and hydrocarbon plays in the Penyu Basin, offshore peninsular Malaysia. *Bulletin. Geological Society of Malaysia*, *68*, 1–23. https://doi.org/10.7186/bgsm68201901

Madon, M., Karim, R. B. A., & Fatt, R. W. H. (1999). Tertiary stratigraphy and correlation schemes. In *The Petroleum Geology and Resources of Malaysia* (pp. 115–137). Petronas.

Madon, M., & Watts, A. B. (1998). Gravity anomalies, subsidence history and the tectonic evolution of the Malay and Penyu Basins (offshore Peninsular Malaysia). *Basin Research*, *10*(4), 375–392. https://doi.org/10.1046/j.1365-2117.1998.00074.x

Madon, M., Yang, J.-S., Abolins, P., Abu Hassan, R., Yakzan, M., & Zainal, S. B. (2006). Petroleum systems of the northern Malay Basin. *Bulletin. Geological Society of Malaysia*, *49*, 125–134. https://doi.org/10.7186/bgsm49200620

Mansor, M. Y., Rahman, A. H. A., Menier, D., & Pubellier, M. (2014). Structural evolution of Malay Basin, its link to Sunda block tectonics. *Marine and Petroleum Geology*, *58*, 736–748. https://doi.org/10.1016/j.marpetgeo.2014.05.003

Matthews, S. J., Fraser, A. J., Lowe, S., Todd, S. P., & Peel, F. J. (1997). Structure, stratigraphy and petroleum geology of the SE Nam con Son Basin, offshore Vietnam. *Geological Society, London, Special Publications*, *126*(1), 89–106. https://doi.org/10.1144/GSL.SP.1997.126.01.07

McGrath, S. M., Clemens, S. C., & Huang, Y. (2023). Pleistocene Sunda shelf submersion-exposure cycles initiate vegetation Walker circulation feedback. *Geology*, *51*, 1053–1056. https://doi.org/10.1130/G51412.1

Metcalfe, I. (2009). Late Palaeozoic and Mesozoic tectonic and palaeogeographical evolution of SE Asia. *Geological Society, London, Special Publications*, *315*(1), 7–23. https://doi.org/10.1144/SP315.2

Metcalfe, I. (2011). Tectonic framework and Phanerozoic evolution of Sundaland. *Gondwana Research*, *19*(1), 3–21. https://doi.org/10.1016/j.gr.2010.02.016

Metcalfe, I. (2017). Tectonic evolution of Sundaland. *Bulletin. Geological Society of Malaysia*, *63*, 27–60. https://doi.org/10.7186/bgsm63201702

Miall, A. D. (2002). Architecture and sequence stratigraphy of Pleistocene fluvial systems in the Malay Basin, based on seismic time-slice analysis. *AAPG Bulletin*, *86*, 1201–1216. https://doi.org/10.1306/61EEDC56-173E-11D7-8645000102C1865D

Molnar, P., & Tapponnier, P. (1975). Cenozoic tectonics of Asia: Effects of a continental collision: Features of recent continental tectonics in Asia can be interpreted as results of the India-Eurasia collision. *Science*, *189*(4201), 419–426. https://doi.org/10.1126/science.189.4201.419

Morley, C. K. (2002). A tectonic model for the tertiary evolution of strike–slip faults and rift basins in SE Asia. *Tectonophysics*, *347*(4), 189–215. https://doi.org/10.1016/S0040-1951(02)00061-6

Morley, C. K. (2012). Late Cretaceous–Early Palaeogene tectonic development of SE Asia. *Earth-Science Reviews*, *115*(1–2), 37–75. https://doi.org/10.1016/j.earscirev.2012.08.002

Morley, C. K. (2016). Major unconformities/termination of extension events and associated surfaces in the South China seas: Review and implications for tectonic development. *Journal of Asian Earth Sciences*, *120*, 62–86. https://doi.org/10.1016/j.jseaes.2016.01.013

Morley, R. J., Morley, H. P., & Restrepo-Pace, P. (2003). Unravelling the tectonically controlled stratigraphy of the West Natuna Basin by means of palaeo-derived mid Tertiary climate changes. *Proceedings, Indonesian Petroleum Association: 29th Annual Convention & Exhibition, October 2003*.

Murray, M. R., & Dorobek, S. L. (2004). Sediment supply, tectonic subsidence, and basin-filling patterns across the southwestern South China Sea during Pliocene to recent time. In P. Clift, W. Kuhnt, P. Wang, & D. Hayes (Eds.), *Geophysical monograph series* (Vol. *149*, pp. 235–254). American Geophysical Union. https://doi.org/10.1029/149GM13

Nayak, S., Masoudi, R., Tarang Patrick Panting, A., BM Diah, M. A., B Roslan, M. R., BM Amin, M. F., R Iyer, S., Aarssen, B. V., Fun, S., & Mishra, S. (2023). Insights on the origin and distribution of CO_2 in Malay Basin, offshore Peninsular Malaysia: A petroleum system modelling approach, IPTC-22832-EA. https://doi.org/10.2523/IPTC-22832-EA

Ng, T. S. (1987). Trap styles of the Tenggol arch and the southern part of the Malay Basin. *Bulletin. Geological Society of Malaysia*, *21*, 177–193. https://doi.org/10.7186/bgsm21198710

Ngah, K., Madon, M., & Tjia, H. D. (1996). Role of pre-tertiary fractures in formation and development of the Malay and Penyu basins. *Geological Society, London, Special Publications*, *106*(1), 281–289. https://doi.org/10.1144/GSL.SP.1996.106.01.18

Petersen, H. I., Mathiesen, A., Fyhn, M. B. W., Dau, N. T., Bojesen-Koefoed, J. A., Nielsen, L. H., & Nytoft, H. P. (2011). Modeling of petroleum generation in the Vietnamese part of the Malay Basin using measured kinetics. *AAPG Bulletin*, *95*(4), 509–536. https://doi.org/10.1306/09271009171

Pubellier, M., & Morley, C. K. (2014). The basins of Sundaland (SE Asia): Evolution and boundary conditions. *Marine and Petroleum Geology*, *58*, 555–578. https://doi.org/10.1016/j.marpetgeo.2013.11.019

Ramli, M. D. (1988). Stratigraphy and palaeofacies development of Carigali's operating areas in the Malay Basin, South China Sea. *Bulletin. Geological Society of Malaysia*, *22*, 153–187. https://doi.org/10.7186/bgsm22198808

Rice-Oxley, E., & Abu-Bakar, A. (2022). Historical and emerging super basins of Southeast Asia. *AAPG Bulletin*, *106*(3), 633–653. https://doi.org/10.1306/09152121048

Rosly, S. F. M., Abdullah, M. S., Bukhari, M. K. A. M., Tazarudin, N., Nawawi, H. A. B. M., Pendkar, N., Panting, A. T. P., Zhou, J., & Torres, J. A. P. (2019). M-70 sand: Realizing the group m hidden opportunity in Malay Basin. *APGCE*, *2019*, 1–5. https://doi.org/10.3997/2214-4609.201903410

Sarr, A.C., Husson, L., Sepulchre, P., Pastier, A.M., Pedoja, K., Elliot, M., Arias-Ruiz, C., Solihuddin, T., Aribowo, S., & Susilohadi. (2019). Subsiding Sundaland. *Geology*, *47*(2), 119–122. https://doi.org/10.1130/G45629.1

Shing, C. Y. (1992). Petrographic and diagenetic studies of the reservoir sandstone of the Malay Basin. *Bulletin. Geological Society of Malaysia*, *32*, 261–283. https://doi.org/10.7186/bgsm32199216

Straume, E. O., Gaina, C., Medvedev, S., Hochmuth, K., Gohl, K., Whittaker, J. M., Abdul Fattah, R., Doornenbal, J. C., & Hopper, J. R. (2019). Globsed: Updated total sediment thickness in the world's oceans. *Geochemistry, Geophysics, Geosystems*, *20*(4), 1756–1772. https://doi.org/10.1029/2018GC008115

Tapponnier, P., Peltzer, G., Le Dain, A. Y., Armijo, R., & Cobbold, P. (1982). Propagating extrusion tectonics in Asia: New insights from simple experiments with plasticine. *Geology*, *10*(12), 611. https://doi.org/10.1130/0091-7613(1982)10<611:PETIAN>2.0.CO;2

Thye, Y. K. (1996). Sequence stratigraphy of the group J, tapis field, Malay Basin. *Warta Geologi (Newsletter of the Geological Society of Malaysia)*, *22*(6), 421–422.

Tingay, M. R., Morley, C., Laird, A. P., Limpornpipat, O., Krisadasima, K., Pabchanda, S., & Macintyre, H. (2011). Overpressures in the northern Malay Basin: Part 1—Origin and distribution. *All Days*, IPTC-15345-MS. https://doi.org/10.2523/IPTC-15345-MS

Tingay, M. R. P., Morley, C. K., Laird, A., Limpornpipat, O., Krisadasima, K., Pabchanda, S., & Macintyre, H. R. (2013). Evidence for overpressure generation by kerogen-to-gas maturation in the northern Malay Basin. *AAPG Bulletin*, *97*(4), 639–672. https://doi.org/10.1306/09041212032

Tjia, H. D. (1994). Inversion tectonics in the Malay Basin: Evidence and timing of events. *Bulletin. Geological Society of Malaysia*, *36*, 119–126.

Tjia, H. D. (1998). Origin and tectonic development of Malay-Penyu-west Natuna basins. *Bulletin. Geological Society of Malaysia*, *42*, 147–160. https://doi.org/10.7186/bgsm42199813

Tjia, H. D. (2014). Wrench-slip reversals and structural inversions: Cenozoic slide-rule tectonics in Sundaland. *Indonesian Journal on Geoscience*, *1*(1), 35–52.

Tjia, H. D., & Liew, K. K. (1996). Changes in tectonic stress field in northern Sunda shelf basins. *Geological Society, London, Special Publications*, *106*(1), 291–306. https://doi.org/10.1144/GSL.SP.1996.106.01.19

Twarog, M. R., Culver, S. J., Mallinson, D. J., Leorri, E., Donovan, B., Harrison, E. I., Hindes, H., Reed, D., Horsman, E., Shazili, N. A. M., & Parham, P. R. (2021). Depositional environments and sequence stratigraphy of post-last glacial maximum incised valley-fill, Malay Basin, northern Sunda shelf. *Marine Geology*, *436*, 106457. https://doi.org/10.1016/j.margeo.2021.106457

Vincelette, R. R., Beaumont, E. A., & Foster, N. H. (1999). Classification of exploration traps. In E. A. Beaumont & N. H. Foster (Eds.), *Exploring for oil and gas traps*. American Association of Petroleum Geologists. https://doi.org/10.1306/TrHbk624C2

Westerhold, T., Marwan, N., Drury, A. J., Liebrand, D., Agnini, C., Anagnostou, E., Barnet, J. S. K., Bohaty, S. M., De Vleeschouwer, D., Florindo, F., Frederichs, T., Hodell, D. A., Holbourn, A. E., Kroon, D., Lauretano, V., Littler, K., Lourens, L. J., Lyle, M., Pälike, H., ... Zachos, J. C. (2020). An astronomically dated record of Earth's climate and its predictability over the last 66 million years. *Science*, *369*(6509), 1383–1387. https://doi.org/10.1126/science.aba6853

Woolands, M. A., & Haw, D. (1976). Tertiary stratigraphy and sedimentation in the Gulf of Thailand. *Offshore South East Asia Conference*, *1976*, 63–84.

Yakzan, M. A., Harun, A., Md Nasib, B., & Morley, R. J. (1996). Integrated biostratigraphic zonation for the Malay Basin. *Bulletin. Geological Society of Malaysia*, *39*, 157–184. https://doi.org/10.7186/bgsm39199615

Yusak, S. A. M. (2012). Sedimentological characterization of deeper group M reservoirs in Malay Basin. *Warta Geologi (Newsletter of the Geological Society of Malaysia)*, *38*(2), 212.

How to cite this article: de Jonge-Anderson, I., Widyanita, A., Busch, A., Doster, F., & Nicholson, U. (2024). New insights into the structural and stratigraphic evolution of the Malay Basin using 3D seismic data: Implications for regional carbon capture and storage potential. *Basin Research*, *36*, e12885. https://doi.org/10.1111/bre.12885